NUCLEAR DATA AND MEASUREMENTS SERIES

ANL/NDM-93

Integral Cross-Section Measurements for $^{7}Li(n,n't)^{4}He$, $^{27}Al(n,p)^{27}Mg$, $^{27}Al(n,a)^{24}Na$, $^{58}Ni(n,p)^{58}Co$, and $^{60}Ni(n,p)^{60}Co$ Relative to ^{238}U Neutron Fission in the Thick-Target $^{9}Be(d,n)^{10}B$ Spectrum at E_d = 7 MeV

by

D.L. Smith, J.W. Meadows, and M.M. Bretscher

October 1985

ARGONNE NATIONAL LABORATORY,
ARGONNE, ILLINOIS 60439, U.S.A.

NUCLEAR DATA AND MEASUREMENTS SERIES

ANL/NDM-93

INTEGRAL CROSS-SECTION MEASUREMENTS FOR $^{7}Li(n,n't)^{4}He$, $^{27}Al(n,p)^{27}Mg$, $^{27}Al(n,\alpha)^{24}Na$, $^{58}Ni(n,p)^{58}Co$ AND $^{60}Ni(n,p)^{60}Co$ RELATIVE TO ^{238}U NEUTRON FISSION IN THE THICK-TARGET $^{9}Be(d,n)^{10}B$ SPECTRUM AT E_d = 7 MeV

by

D. L. Smith, J. W. Meadows and M. M. Bretscher

October 1985

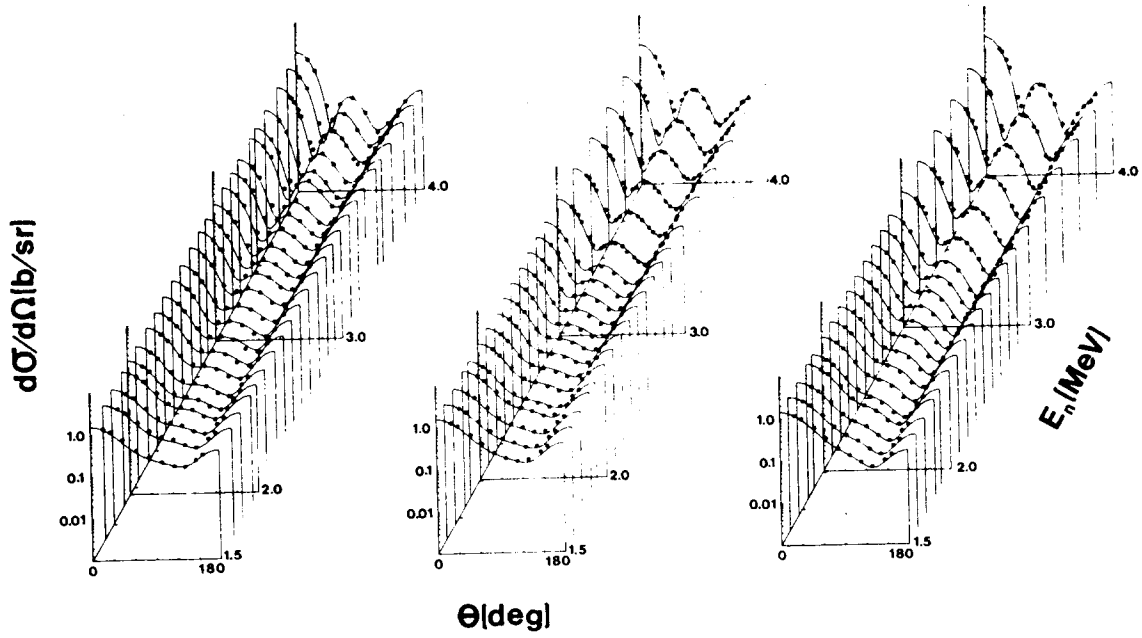

ARGONNE NATIONAL LABORATORY, ARGONNE, ILLINOIS

Operated by THE UNIVERSITY OF CHICAGO

for the U. S. DEPARTMENT OF ENERGY

under Contract W-31-109-Eng-38

Argonne National Laboratory, with facilities in the states of Illinois and Idaho, is owned by the United States government, and operated by The University of Chicago under the provisions of a contract with the Department of Energy.

DISCLAIMER

This report was prepared as an account of work sponsored by an agency of the United States Government. Neither the United States Government nor any agency thereof, nor any of their employees, makes any warranty, express or implied, or assumes any legal liability or responsibility for the accuracy, completeness, or usefulness of any information, apparatus, product, or process disclosed, or represents that its use would not infringe privately owned rights. Reference herein to any specific commercial product, process, or service by trade name, trademark, manufacturer, or otherwise, does not necessarily constitute or imply its endorsement, recommendation, or favoring by the United States Government or any agency thereof. The views and opinions of authors expressed herein do not necessarily state or reflect those of the United States Government or any agency thereof.

ANL/NDM-93

INTEGRAL CROSS-SECTION MEASUREMENTS FOR $^{7}Li(n,n't)^{4}He$, $^{27}Al(n,p)^{27}Mg$, $^{27}Al(n,\alpha)^{24}Na$, $^{58}Ni(n,p)^{58}Co$ AND $^{60}Ni(n,p)^{60}Co$ RELATIVE TO ^{238}U NEUTRON FISSION IN THE THICK-TARGET $^{9}Be(d,n)^{10}B$ SPECTRUM AT E_d = 7 MeV*

by

D. L. Smith, J. W. Meadows and M. M. Bretscher

October 1985

E

NUCLEAR REACTIONS $^{7}Li(n,n't)^{4}He$, $^{27}Al(n,p)^{27}Mg$, $^{27}Al(n,\alpha)^{24}Na$, $^{58}Ni(n,p)^{58}Co$ and $^{60}Ni(n,p)^{60}Co$. Measured integral σ relative to $^{238}U(n,f)$ in Thick-target $^{9}Be(d,n)^{10}B$ Spectrum at E_d = 7 MeV. Integral/differential comparison with evaluated differential σ results. Discussion of the methodology.

Applied Physics Division
Argonne National Laboratory
9700 South Cass Avenue
Argonne, Illinois 60439
USA

*This work supported by the U.S. Department of Energy.

NUCLEAR DATA AND MEASUREMENTS SERIES

The Nuclear Data and Measurements Series presents results of studies in the field of microscopic nuclear data. The primary objective is the dissemination of information in the comprehensive form required for nuclear technology applications. This Series is devoted to: a) measured microscopic nuclear parameters, b) experimental techniques and facilities employed in measurements, c) the analysis, correlation and interpretation of nuclear data, and d) the evaluation of nuclear data. Contributions to this Series are reviewed to assure technical competence and, unless otherwise stated, the contents can be formally referenced. This Series does not supplant formal journal publication but it does provide the more extensive information required for technological applications (e.g., tabulated numerical data) in a timely manner.

INFORMATION ABOUT OTHER ISSUES IN THE ANL/NDM SERIES:

A list of titles and authors for reports ANL/NDM-1 through ANL/NDM-50 can be obtained by referring to any report of this series numbered ANL/NDM-51 through ANL/NDM-76. Requests for a complete list of titles or for copies of previous reports should be directed to:

Section Secretary
Applied Nuclear Physics Section
Applied Physics Division
Building 316
Argonne National Laboratory
9700 South Cass Avenue
Argonne, Illinois 60439
USA

ANL/NDM-51 Measured and Evaluated Neutron Cross Sections of Elemental Bismuth by A. Smith, P. Guenther, D. Smith and J. Whalen, April 1980.

ANL/NDM-52 Neutron Total and Scattering Cross Sections of ^{6}Li in the Few MeV Region by P. Guenther, A. Smith and J. Whalen, February 1980.

ANL/NDM-53 Neutron Source Investigations in Support of the Cross Section Program at the Argonne Fast-Neutron Generator by James W. Meadows and Donald L. Smith, May 1980.

ANL/NDM-54 The Nonelastic-Scattering Cross Sections of Elemental Nickel by A. B. Smith, P. T. Guenther and J. F. Whalen, June 1980.

ANL/NDM-55 Thermal Neutron Calibration of a Tritium Extraction Facility using the $^{6}Li(n,t)^{4}He/^{197}Au(n,\gamma)^{198}Au$ Cross Section Ratio for Standardization by M. M. Bretscher and D. L. Smith, August 1980.

ANL/NDM-56 Fast-Neutron Interactions with ^{182}W, ^{184}W and ^{186}W by P. T. Guenther, A. B. Smith and J. F. Whalen, December 1980.

ANL/NDM-57 The Total, Elastic- and Inelastic-Scattering Fast-Neutron Cross Sections of Natural Chromium by Peter T. Guenther, Alan B. Smith and James F. Whalen, January 1981.

ANL/NDM-58 Review of Measurement Techniques for the Neutron Capture Process by W. P. Poenitz, August 1981.

ANL/NDM-59 Review of the Importance of the Neutron Capture Process in Fission Reactors by Wolfgang P. Poenitz, July 1981.

ANL/NDM-60 Gamma-Ray Detector Calibration Methods Utilized in the Argonne FNG Group Activation Cross Section Measurement Program by James W. Meadows and Donald L. Smith, April 1984.

ANL/NDM-61 Fast-neutron Total and Scattering Cross Sections of ^{58}Ni by Carl Budtz-Jørgensen, Peter T. Guenther, Alan B. Smith and James F. Whalen, September 1981.

ANL/NDM-62 Covariance Matrices and Applications to the Field of Nuclear Data by Donald L. Smith, November 1981.

ANL/NDM-63 On Neutron Inelastic-Scattering Cross Sections of ^{232}Th, ^{233}U, ^{235}U, ^{238}U, ^{239}U, and ^{239}Pu and ^{240}Pu by Alan B. Smith and Peter T. Guenther, January 1982.

ANL/NDM-64 The Fission-Fragment Angular Distributions and Total Kinetic Energies for ^{235}U(n,f) from 0.18 to 8.83 MeV by James W. Meadows and Carl Budtz-Jørgensen, January 1982.

ANL/NDM-65 Note on the Elastic Scattering of Several-MeV Neutrons from Elemental Calcium by Alan B. Smith and Peter T. Guenther, March 1982.

ANL/NDM-66 Fast-neutron Scattering Cross Sections of Elemental Silver by Alan B. Smith and Peter T. Guenther, May 1982.

ANL/NDM-67 Non-evaluation Applications for Covariance Matrices by Donald L. Smith, July 1982.

ANL/NDM-68 Fast-neutron Total and Scattering Cross Sections of ^{103}Rh by Alan B. Smith, Peter T. Guenther and James F. Whalen, July 1982.

ANL/NDM-69 Fast-neutron Scattering Cross Sections of Elemental Zirconium by Alan B. Smith and Peter T. Guenther, December 1982.

ANL/NDM-70 Fast-neutron Total and Scattering Cross Sections of Niobium by Alan B. Smith, Peter T. Guenther and James F. Whalen, July 1982.

ANL/NDM-71 Fast-neutron Total and Scattering Cross Sections of Elemental Palladium by Alan B. Smith, Peter T. Guenther and James F. Whalen, June 1982.

ANL/NDM-72 Fast-neutron Scattering from Elemental Cadmium by Alan B. Smith and Peter T. Guenther, July 1982.

ANL/NDM-73 Fast-neutron Elastic-Scattering Cross Sections of Elemental Tin by C. Budtz-Jørgensen, Peter T. Guenther and Alan B. Smith, July 1982.

ANL/NDM-74 Evaluation of the ^{238}U Neutron Total Cross Section by Wolfgang Poenitz, Alan B. Smith and Robert Howerton, December 1982.

ANL/NDM-75 Neutron Total and Scattering Cross Sections of Elemental Antimony by A. B. Smith, P. T. Guenther and J. F. Whalen, September 1982.

ANL/NDM-76 Scattering of Fast-Neutrons from Elemental Molybdenum by Alan B. Smith and Peter T. Guenther, November 1982.

ANL/NDM-77 A Least-Squares Method for Deriving Reaction Differential Cross Section Information from Measurements Performed in Diverse Neutron Fields by Donald L. Smith, November 1982.

ANL/NDM-78 Fast-Neutron Total and Elastic-Scattering Cross Sections of Elemental Indium by A. B. Smith, P. T. Guenther, and J. F. Whalen, November 1982.

ANL/NDM-79 Few-MeV Neutrons Incident on Yttrium by C. Budtz-Jørgensen, P. Guenther, A. Smith and J. Whalen, June 1983.

ANL/NDM-80 Neutron Total Cross Section Measurements in the Energy Region from 47 keV to 20 MeV by W. P. Poenitz and J. F. Whalen, July 1983.

ANL/NDM-81 Covariances for Neutron Cross Sections Calculated Using a Regional Model Based on Elemental-Model Fits to Experimental Data by D. L. Smith and P. T. Guenther, November 1983.

ANL/NDM-82 Reaction Differential Cross Sections from the Least-Squares Unfolding of Ratio Data Measured in Diverse Neutron Fields by D. L. Smith, January 1984.

ANL/NDM-83 The Fission Cross Sections of Some Thorium, Uranium, Neptunium and Plutonium Isotopes Relative to ^{235}U by J. W. Meadows, October 1983.

ANL/NDM-84 ^{235}U and ^{239}Pu Sample-Mass Determinations and Intercomparisons by W. P. Poenitz and J. W. Meadows, November 1983.

ANL/NDM-85 Measurement of the $^{51}V(n,p)^{51}Ti$ Reaction Cross Section from Threshold to 9.3 MeV by the Activation Method by D. L. Smith, J. W. Meadows and I. Kanno, June 1984.

ANL/NDM-86 Energy-Differential Cross Section Measurement for the $^{51}V(n,\alpha)^{48}Sc$ Reaction by I. Kanno, J. W. Meadows, and D. L. Smith, July 1984.

ANL/NDM-87 Cross-Section Measurement for the $^{7}Li(n,n't)^{4}He$ Reaction at 14.74 MeV by D. L. Smith, J. W. Meadows, M. M. Bretscher and S. A. Cox, September 1984.

ANL/NDM-88 An Evaluated Nuclear Data File for Niobium by A. B. Smith, D. L. Smith and R. J. Howerton, March 1985.

ANL/NDM-89 Compilation and Evaluation of 14-MeV Neutron Activation Cross Sections for Nuclear Technology Applications: Set I by Bernard P. Evain, Donald L. Smith and Paul Lucchese, April 1985.

ANL/NDM-90 Fast-Neutron-Spectrum Measurements for the Thick-Target $^{9}Be(d,n)^{10}B$ Reaction at E_d = 7 MeV by D. L. Smith, J. W. Meadows and P. T. Guenther, April, 1985.

ANL/NDM-91 On The Energy-Dependence of the Optical-Model of Neutron Scattering from Niobium by A. B. Smith, P. T. Guenther and R. D. Lawson, May 1985.

ANL/NDM-92 Nuclear Data Uncertainties, Volume I: Basic Concepts of Probability by Donald L. Smith, April 1986.

TABLE OF CONTENTS

	Page
ABSTRACT	vii
I. INTRODUCTION	1
II. EXPERIMENTAL PROCEDURE	3
A. Neutron Production	3
B. Samples and Fission Monitor	4
C. Irradiation Procedure	5
D. Sample-Activity Measurements	7
III. DATA ANALYSIS AND RESULTS	9
A. Fission-Data Processing	9
B. Sample-Activity Data Processing	10
C. Neutron-Scattering Corrections	11
D. Experimental Cross-Section Ratio Determinations	12
E. Experimental Errors	13
F. Experimental Results	16
IV. INTEGRAL/DIFFERENTIAL ANALYSIS AND COMPARISONS	19
A. Calculated Integral Cross-Section Ratios and Errors	19
B. Comparison of Experimental and Calculated Results	20
V. DISCUSSION OF THE METHOD AND CONCLUSIONS	22
VI. SUMMARY	24
ACKNOWLEDGEMENTS	25
APPENDICES	26
A. Procedure for Deriving Experimental Integral Neutron-Activation Cross-Section Ratios	26
B. Procedure for Deriving Neutron-Scattering Corrections	52
C. Procedure for Deriving Errors in Calculated Integral Neutron-Activation Cross-Section Ratios	53
REFERENCES	57
TABLES	61
FIGURES	90

INTEGRAL CROSS-SECTION MEASUREMENTS FOR $^{7}Li(n,n't)^{4}He$, $^{27}Al(n,p)^{27}Mg$, $^{27}Al(n,\alpha)^{24}Na$, $^{58}Ni(n,p)^{58}Co$ AND $^{60}Ni(n,p)^{60}Co$ RELATIVE TO ^{238}U NEUTRON FISSION IN THE THICK-TARGET $^{9}Be(d,n)^{10}B$ SPECTRUM AT E_d = 7 MeV*

by

D. L. Smith, J. W. Meadows and M. M. Bretscher

Applied Physics Division
Argonne National Laboratory
9700 South Cass Avenue
Argonne, Illinois 60439
USA

ABSTRACT

Integral activation cross sections for the reactions $^{7}Li(n,n't)^{4}He$, $^{27}Al(n,p)^{27}Mg$, $^{27}Al(n,\alpha)^{24}Na$, $^{58}Ni(n,p)^{58}Co$ and $^{60}Ni(n,p)^{60}Co$ have been measured relative to the ^{238}U neutron-fission cross section in the neutron field produced by 7-MeV deuteron bombardment of a thick beryllium target. The measured results are compared with calculated values derived using ENDF/B-V differential cross sections and published spectral information. In all instances, these experimental results appear to be very consistent with the predictions of ENDF/B-V. Details of the experimental and analytical procedures are documented, and the potential of this integral method in neutron nuclear data development applications is discussed.

---

*This work supported by the U.S. Department of Energy.

I. INTRODUCTION

Historically, the development of neutron-activation cross section data for nuclear-energy applications has involved both differential and integral studies. Differential cross-section results are generally obtained from measurements using nearly monoenergetic neutron fields produced at accelerator facilities, while integral measurements are usually performed using fission-neutron fields. Nuclear-model calculations are also used to supplement monoenergetic measurements. The results of such calculations can then be tested via integral studies. An active area of research in this field is the quest for, and elimination of, discrepancies between corresponding differential and integral results.

It has been pointed out that useful integral (or broad-energy) neutron spectra can be produced by the bombardment of thick, light-element targets with monoenergetic protons and deuterons (e.g., Refs. 1-6), and that worthwhile neutron cross-section information can be derived from measurements in these spectra (e.g., Refs. 7 and 8). Furthermore, it has been shown (e.g., Ref. 9) that if nuclear data development is approached in such a way that the processes of measurement and evaluation are unified, then there need not be a sharp distinction between differential and integral information. Since data from monoenergetic measurements are easier to interpret, however, such measurements are generally preferable whenever they are feasible. The most significant shortcomings of monoenergetic-measurement methods are limited energy scope and neutron intensity. Certain integral sources (including those produced at accelerators) can yield much higher intensity levels than are practical for monoenergetic fields. They also offer the potential for addressing the energy range 10 - 14 MeV which cannot be conveniently accessed with monoenergetic sources. There is a strong current interest in obtaining data in this particular neutron energy range for fusion-energy applications, particularly for long-half-life or low-yielding activation reactions (e.g., Ref. 10). Intense neutron sources can be very useful for such measurements.

Accurate integral-cross-section measurements are not as simple to perform as monoenergetic measurements, since sophisticated correction procedures are required. This fact has not been as widely appreciated as it should be. We have been exploring this matter at our own laboratory (e.g., Refs. 9 and 11) and elsewhere via collaborations (e.g., Refs. 12-14). An essential requirement for such measurements, and for interpretation of the experimental integral data, is detailed and precise knowledge of the neutron field in which the measurements are to be performed. For accelerator sources this entails knowledge of the neutron emission energy and angular distributions. In spite of the fact that this knowledge can, in principle, be readily obtained from time-of-flight (TOF) experiments, the desired

information is generally not available. The difficulty of accurately calibrating detectors for TOF measurements is one of several reasons for the paucity of this type of information. The neutron spectrum produced by 7-MeV deuteron bombardment of a thick beryllium target has been investigated in some detail at CBNM-Geel [12] and at our own laboratory [11]. Therefore, it is reasonable to consider using it for integral investigations of the type described above.

The present research effort involves the development of reliable measurement and analysis procedures needed to conduct integral activation cross-section investigations with accelerator sources such as the $^{9}Be(d,n)^{10}B$ thick-target reaction. These procedures are tested via consideration of some selected reactions of interest for fusion-energy applications. Neutron-induced fission of ^{238}U is chosen as the basic monitor reaction for this work because its cross section appears to be quite well known over the response range of the present integral spectrum [15,16]. The $^{58}Ni(n,p)^{58}Co$ reaction is also thought to be rather well known over most of the present integral response range. The reactions $^{27}Al(n,p)^{27}Mg$ and $^{27}Al(n,\alpha)^{24}Na$ are moderately well-known over the present integral response range and their responses to the integral spectrum are at somewhat higher energy than the two previously-mentioned reactions. Knowledge of the differential cross sections for $^{7}Li(n,n't)^{4}He$ and $^{60}Ni(n,p)^{60}Co$ over their response ranges in the present spectrum is considered to be less certain. The $^{7}Li(n,n't)^{4}He$ reaction is important to fusion energy from the point of view of tritium fuel breeding while the proton and alpha-particle emission reactions are relevant to dosimetry and radiation-damage concerns [10]. The present investigation thus serves to test the measurement and data-analysis procedures against reasonably well-known reaction cross sections, and to provide valuable information relevant to two less-well-understood reaction processes. This investigation also seeks to further examine the suitablility of the $^{9}Be(d,n)^{10}B$ thick-target reaction at E_d = 7 MeV for neutron cross-section data-development purposes in the MeV neutron-energy range, and to determine whether the current knowledge of the neutron-emission spectrum at E_d = 7 MeV is adequate for applications of this nature.

Experimental procedures are described in Chapter II while data-analysis procedures are discussed in Chapter III. The experimental results are also presented in Chapter III. Chapter IV deals with the generation of calculated integral results to compare with experiment, and with the outcome of this comparison. The usefulness of the method is assessed in Chapter V. Certain analytical procedures involved in the application of this method are documented in appendices to this report.

II. EXPERIMENTAL PROCEDURE

The basic method employed in this experiment is as follows: Thin cylindrical sample discs were attached, one at a time, to a low-mass fission chamber containing a calibrated, depleted-uranium deposit. This assembly was placed close to a thick beryllium target on a beam line of the Argonne National Laboratory Fast-Neutron Generator (FNG). Fast neutrons were produced by bombarding the beryllium target with 7-MeV deuterons. Tritium was extracted from the irradiated lithium samples by vaporizing them in a furnace and then converting the released tritium, and hydrogen carrier gas, to water. Collected water samples were counted by the liquid-scintillation method to assay their tritium content. Other irradiated samples were gamma-ray counted using calibrated Ge(Li) detectors in order to measure the ^{24}Na, ^{27}Mg, ^{58}Co and ^{60}Co activities of interest in the present investigation. The measured data were ultimately converted to activation-cross-section ratios relative to the ^{238}U neutron-fission reaction, following the application of various corrections. Several details of this procedure are discussed in the remainder of this chapter, while pertinent references to previous work from this laboratory are provided to cover aspects not treated extensively in this report.

A. Neutron Production

As indicated above, the FNG accelerator was employed as a source of nearly monoenergetic 7-MeV deuterons [17]. The target assembly was situated at a station located on the axis of the accelerator during the present experiment. Continuous magnetic analysis of the deuteron beam during the irradiations was therefore not possible so the following procedure was employed: Calibration of the deuteron-beam energy was based upon prior magnetic analysis and threshold measurements for the $^{7}Li(p,n)^{7}Be$ and $^{11}B(p,n)^{11}C$ reactions [18]. These prior measurements were made at another target station which can utilize precision magnetic beam-analysis apparatus. Stability of the beam energy on target for the station actually used to acquire the present data was monitored by measuring the accelerator terminal potential. The uncertainty in this process was the main source of error in defining the beam energy. Overall, it was concluded that the deuteron-beam energy remained in the range 7.00 ± 0.03 MeV for the entire experiment. Variations in the neutron emission spectrum over this narrow range are of little consequence in the present context.

The $^{9}Be(d,n)^{10}B$ reaction has a Q-value of + 4.362 MeV [19]. For 7-MeV incident deuterons, the emitted neutrons have energies < 11.4 MeV.

The neutron-emission spectrum for thick-target (incident deuterons are stopped in the beryllium) bombardment is defined quantitatively in Refs. 11 and 12. The range of 7-MeV deuterons in beryllium metal is ~ 250 μm [20]. The present target assembly is shown schematically in Fig. 1. A 0.050-cm-thick pure beryllium-metal disk is used as the target element for this assembly, thus assuring stoppage of the incident deuterons. The rest of the target assembly is fabricated of copper for good heat dissipation and it is water cooled. This target assembly is designed to present a low mass in the vicinity of the beam spot (while preserving the requirements for structural integrity and cooling). The intent is to minimize neutron-scattering perturbations to the primary spectrum. This assembly seems to be capable of dissipating at least 100 watts of beam power. Owing to the high neutron output from this target, it was necessary to temporarily surround the entire target and detector with massive amounts of shielding material for radiation safety purposes. The shielding was stacked so as to create an irradiation cavity in which the distance from the walls to the target was ~ 1 m. The shielding material used was mostly hydrogenous (e.g., concrete and polyethelene blocks). However, the inner walls of the cavity were lined with cadmium in order to reduce thermal-neutron return from the shielding. This return could induce troublesome background activities in the irradiated samples.

B. Samples and Fission Monitor

Isotopic ^{7}Li samples were fabricated from chemically-pure (99.92%) lithium metal in the form of wafers 1.9-cm in diameter and roughly 0.6 cm thick. The fabrication process was carried out in a glove box filled with inert argon gas. Each wafer was enclosed in an air-tight aluminum capsule with ~ 0.5 mm thick walls. These capsules prevented the lithium from reacting with the atmosphere (mainly with water vapor) and kept tritium from escaping after the irradiations. The samples were fabricated about 3 years prior to this experiment. Their weights at the time of this experiment differed by < 0.1 mg from those recorded at the time of fabrication. Furthermore, each sample used passed two leak tests with pressurized helium (3 years apart). These indicators provided confidence that no cladding failures were involved in this experiment. The ^{7}Li-enriched material (a ^{7}Li-to-^{6}Li ratio of 1511) was obtained from the Stable Isotopes Division, Oak Ridge National Laboratory [21]. Table I from Ref. 22 gives specific information on this material (Batch No. ORNL 4731100). This reference also provides a detailed exposition of the sample fabrication process which, therefore, will not be repeated here. Four distinct samples were employed in the present work. Three were irradiated in independent exposures while a fourth unirradiated one helped to check the extraction/counting process for possible background and tritium-contamination effects. Parameters for these samples are documented in Table 1.

Two different types of samples were used in measurements for the aluminum and nickel reactions. Four nearly identical nickel-aluminum

alloy samples were provided by the Central Bureau of Nuclear Measurements, Geel, Belgium. They were fabricated via a process involving HF levitation melting, followed by rolling and machining to achieve uniformity. These samples contain (2.00 ± 0.02) wt% pure aluminum. The rest of the material in each of them is pure elemental nickel. A fifth sample was fabricated at Argonne National Laboratory. It consists of alternating layers of pure aluminum foil (0.00254-cm thick each) and pure nickel foil (0.03048-cm thick each). There are six layers of each element. The aluminum content of this sample amounts to 2.52 wt%. The layers are held together by Eastman Kodak Corporation 910 adhesive compound [23]. The mass of the dried adhesive material was determined to be < 0.1 g. Parameters for these samples are documented in Table 2.

The fission monitor is a low-mass, parallel-plate ionization flow counter used to detect fission fragments emitted from a thin deposit of uranium (see Fig. 1). The chamber itself has 0.0254-cm-thick steel walls. The chamber electrode and uranium-deposit backing are 0.0254-cm-thick steel disks. Methane (CH_4) at atmospheric pressure was used as the gaseous medium in this experiment. The uranium deposit (U-deposit) consists of a thin, uniform film of depleted uranium (effectively 100% ^{238}U) 2.54-cm in diameter, amounting to 5.009×10^{18} (±2%) atoms. Procedures for making and calibrating this deposit are described elsewhere [24-26].

C. Irradiation Procedure

The first part of this experiment consisted of measurements intended to explore the possible effects of scattered neutrons from the above-mentioned shielding. This was accomplished by means of TOF-spectrum measurements, with the fission chamber placed at a position ~ 10 cm from the target. It was found that the number of ^{238}U fissions which could be attributed to neutrons backscattered from the shielding was negligible. Since all the other reactions involved in this experiment have effective thresholds of-the-order-of or higher than ^{238}U fission, it was concluded that neutron return from the shielding could be neglected from the point of view of radioactivity production which might affect the present work.

All additional measurements were performed without regard to neutron TOF. The sample irradiations were conducted at three distances from the neutron source: ~ 6 cm, ~ 8 cm and ~ 10 cm. These three different geometric configurations were considered in order to check the data correction procedures. The irradiations ranged from ~ 20 m to ~ 13 h in duration.

The Fission-event signals were processed with a multichannel analyzer. They were also analyzed with a pulse selector and scaler for backup. For the latter, signals with amplitudes above a selected level were accepted as the fission-count data. This bias level was set in order to reject alpha-particle events, recoil-proton events from neutron interaction with hydrogen in the methane gas, and electronic noise. Information required to calculate a correction for extrapolation of the fission spectrum to

zero pulse height was also acquired for each run.

When this experiment first began, it was noticed that the shape of the recorded fission spectrum would experience noticeable degradation whenever the incident deuteron-beam current was raised above a certain level. In particular, the quality of separation of the alpha-particle events from the fission events tended to deteriorate. It was concluded that this effect could be attributed to pulse pileup in the fission-detector preamplfier. The high-intensity neutron field from the $^{9}Be(d,n)^{10}B$ thick-target reaction produces copious low-level pulses in the ionization chamber. Many of these are due to recoiling protons from the methane filler gas. Whenever the capacity of the preamplifier to process individual pulses is exceeded, a distored spectrum will result. Since such pulse overloading can also lead to recording-system deadtime which is not indicated by the multi-channel analyzer, it was evident that this problem warranted more detailed investigation prior to irradiation of the specially-prepared experimental samples. The fission detector was placed ~ 10 cm from the target for this particular study. A pulser signal was introduced at the "TEST" input of the detector preamplifier. The signal amplitude was adjusted so that it would appear as a peak in the spectrum, isolated from events produced by fissions and alpha particles. A series of measurements was carried out using various deuteron beam-current levels. The pulser peak yield per unit of measurement livetime (for the multichannel used to record the data) was determined. This parameter was found to decrease measurably for beam currents above ~ 7μA. At 12μA, this decrease amounted to ~ 3%. Furthermore, distinct distortion of the pulser-peak shape was observed in conjunction with decreased detection efficiency, thus clearly demonstrating the spectrum-shape degradation mechanism discussed above. For irradiations performed at ~ 6 cm and ~ 8 cm, the tolerable beam-current levels are evidently even lower. We did not perform explicit measurements to determine these limits. However, it was estimated that at ~ 6 cm, the onset of the effect should be observed at ~ 2.5 μA, while at ~ 8 cm it would be apparent at ~ 4.5 μA. It was thus decided to limit the incident beam current to ~ 3.5 μA for all the irradiations. The pulse-pileup problem was then essentially negligible, except possibly for irradiations at the 6-cm distance. For these close-in exposures, the fission losses were estimated to amount to < 2%. Since the required correction for the 6-cm measurements was not explicitly determined, and since the 2% estimate represents an upper bound, it was assumed that the fission losses amounted to ~ 1% for these close-in irradiations. However, it was noticed that none of the spectra recorded during the actual sample-irradiation runs showed any noticeable signs of shape degradation.

In addition to the fission events, the integrated beam charge and pulses from a long counter (LC) were recorded during each irradiation. The LC was placed in a fixed position outside the shielded target area where it monitored neutron leakage through the shielding. The geometry of the experiment was stable, so the neutron leakage provided a fairly reliable relative monitor of neutron production from the target during the experiment. The beryllium target exhibited a very stable level of neutron production during the course of this experiment. Also, it showed no visible signs of deterioration by the end of the experiment.

D. Sample-Activity Measurements

The activity determinations for the irradiated lithium samples differed profoundly from those for the nickel-aluminum samples. Therefore, the two procedures will be discussed separately. The pertinent decay properties for reaction products of interest in the present experiment are summarized in Table 3.

Tritium Activities of the Lithium Samples:

The procedure used for extracting tritium from the irradiated lithium samples has been described in detail in previous publications from this laboratory [22,27-29]. An isotopic-dilution method using normal hydrogen as the carrier gas was used. An irradiated lithium sample (in its Al capsule) was placed in the chamber of a furnace. The system was evacuated and a precise quantity of ultra-pure (99.999%) hydrogen was added from a calibrated reservoir. The sample was then heated to a temperature above the dissociation temperature of LiH and LiT. The released T and H were passed through a freshly-activated CuO column where they were converted to water vapor. The water sample was collected in an evacuated pyrex flask maintained at liquid-nitrogen temperature. After weighing, the sample was transferred to and flame-sealed in a glass ampoule. The extraction apparatus was thoroughly cleaned prior to each individual extraction process to minimize contamination problems. Furthermore, the lithium-sample extractions were interspersed with the generation of water samples from pure hydrogen alone (no lithium sample). Finally, the unirradiated sample was also processed through this system as a control. Calculations were performed to determine what fraction of the hydrogen gas introduced in this dilution process was recovered in the water samples. Normally $\lesssim 6$ grams of water were collected for a typical sample, and $\lesssim 1\%$ of the hydrogen introduced into the system was lost. It is assumed that the recovery fraction for tritium is about the same as for hydrogen. This hypothesis has been confirmed in this laboratory, and through intercomparison with techniques from other laboratories (e.g., Refs. 27 and 29).

The activities of the extracted-water samples were determined by liquid-scintillation counting using an apparatus that is commercially available [30]. The procedure is described in Refs. 27 and 29. Substandards for calibration of this facility were prepared from the NBS tritiated-water primary standard SRM 4926-C [31]. The activity of the NBS standard is quoted as 3406 (± 0.6%) dps/g on September 3, 1978. However, this value has been revised upward by 0.7% to 3430 dps/g (with the same error) based on recent work at Rockwell International Corporation (Refs. 29 and 32). An efficiency of 37.02% for the present tritium-counting system was based on these recent results. The data were corrected for the nearly-constant background level of the counting system. Table 4 summarizes the major parameters associated with the tritium extraction and counting procedures. Note that the calculated water-sample masses m(C) (based on the carrier hydrogen introduced into the system) and the measured sample masses m(E) differ by ~ 1.1-2.0%. The data were corrected for this effect. The overall fidelity of the tritium-extraction and tritium-counting processes has been examined in detail via measurements for $^{6}Li(n,t)^{4}He$ alone, as discussed in Refs. 27 and 29.

Gamma-Ray Activities of the Nickel-Aluminum Samples:

Information needed to obtain reaction cross section results for each of the irradiated nickel-aluminum samples was acquired by gamma-ray counting with Ge(Li) detectors. Our gamma-ray calibration and counting procedures have been reported [33]. The present experiment employed both coincidence-counting methods and measurements relative to standard sources for calibration. Acceptable consistency was obtained for the various calibation procedures used. The activities of interest were: ^{24}Na, ^{27}Mg, ^{58}Co and ^{60}Co. As indicated in Table 3, ^{24m}Na, ^{58m}Co and ^{60m}Co activities were also produced by the irradiations, and they had to be dealt with. In each instance the sample counts were delayed for suitably long periods to insure that these isomer activities had decayed entirely to their respective ground states. Thus, the measured cross-section results include both the isomer and ground-state reaction contributions (see Table 3).

Only one sample, CBNM Ni-Aℓ No. 1 (Table 2), was used to investigate the $^{27}Aℓ(n,p)^{27}Mg$ reaction. The half life of ^{27}Mg is much shorter than those for any of the other measured activities (see Table 3). Data relevant to the other reactions considered for aluminum and nickel were obtained from each of the remaining four samples listed in Table 2. These samples were first counted to deduce their ^{24}Na activities. Several days later, counting for ^{58}Co was undertaken. ^{58}Co activity

interferes with ^{60}Co counting because the 1.322-MeV sum-peak line (0.511-MeV β^+ annihilation gamma rays and 0.811-MeV gamma rays) from ^{58}Co is close to the 1.333-MeV ^{60}Co gamma-ray line. Thus, the ^{60}Co activity measurements were deferred until two years after the sample irradiations. By then, the ^{58}Co sum-peak yields were vastly reduced, though they were still observable. Finally, the samples were counted once again three years after the irradiations. This time there was no evidence of any residual ^{58}Co sum-peak yield to interfere with the ^{60}Co measurements.

III. DATA ANALYSIS AND RESULTS

The processing of raw experimental data was divided into several distinct steps. First, the fission-detector data were analyzed. This included spectrum summing and the application of several corrections. The consistency of the fission, beam-current integrator and long-counter data was also examined. Next, the sample-activity data were analyzed. The procedure for the lithium samples was quite distinct from that for the nickel-aluminum samples, though in each case consideration of detector efficiencies and correction for activity decay were important aspects. Corrections for geometry, radiation absorption, neutron-source properties and neutron multiple scattering were evaluated by means of a computer. These diverse results were then combined to produce cross-section-ratio values. Errors in these ratios were estimated from uncertainty information for the component parameters. Finally, comparable data were averaged by a least-squares method in order to obtain single values for each reaction.

A. Fission-Data Processing

All the fission spectra were summed above their α-event cutoff levels. Corrections for fission events masked by the α events and other low-pulse-height signals were estimated by extrapolating the flat portions of the fission spectra just above the α events. These corrections amounted to ~ 3.3%, and they led to an increase in the recorded fissions. Fission fragments emitted within the U-deposit near 90 degrees relative to the incident neutrons cannot escape the deposit and are thus not observed. A correction for this effect was calculated using previously-described methods [24]. This correction produced an increase in fissions which was found to be ~ 3.3%. Fission events were also lost due to multi-channel-analyzer deadtime effects. These losses were in the range 0.5 - 1.2%, so suitable corrections were applied. As indicated in Chapter II, the losses due to preamplifier pileup effects were found to be negligible except for measurements at the 6-cm position, where a correction of ~ 1% was estimated to be necessary.

With one exception, the fission detector, current integrator and long-counter data were found to be consistent. That single exception was traced to a misrecording of the long-counter counts for one of the runs, and it was thus of no serious consequence.

B. Sample-Activity Data Processing

The only feature which the activity data analyses for the lithium samples and nickel-aluminum samples share is that of correcting for the decay of activity in the samples following irradiation. Half-life values from Table 3 were used, and the procedure itself is described in Ref. 34. Other aspects of the activity analyses are discussed separately below.

Tritium Activities of the Lithium Samples:

The pertinent parameters deduced by liquid-scintillation-counting of tritium extracted from the irradiated lithium samples appear in Table 4. It was determined from an examination of sample ^{7}Li No. 15, and from other background studies, that the lithium samples were not contaminated with tritium prior to irradiation, and furthermore that the tritium-extraction apparatus was free of spurious contamination. An upper limit on such contamination effects was placed at 0.2% for the most-weakly irradiated sample, namely ^{7}Li No. 11. The total number of tritium atoms produced in each of the three irradiated samples was obtained by multiplying the lithium mass (Table 4, 2nd column) by the corrected value of distintegrations of tritium per sec per gram of lithium (Table 4, 4th column), and then multiplying this product by an additional factor to account for the decay of tritium prior to counting of the samples.

Gamma-Ray Activities of the Nickel-Aluminum Samples:

With one exception, the irradiated samples were each counted several times for the following gamma-ray activities: ^{24}Na from the $^{27}Al(n,\alpha)^{24}Na$ reaction, ^{58}Co from the $^{58}Ni(n,p)^{58}Co$ reaction, and ^{60}Co from the $^{60}Ni(n,p)^{60}Co$ reaction. The exception was ^{27}Mg from the $^{27}Al(n,p)^{27}Mg$ reaction. Just one sample was counted for this activity, namely CBNM Ni-Al No. 1 (Table 2), and it was counted only once because of the short decay half life of ^{27}Mg (Table 3). Several detector configurations were involved. Each counting configuration was reproducible, and calibration stability was monitored periodically using standard sources. From these repeated counts it was deduced that the counting results were not significantly affected by the orientation of the samples (i.e., which face of the sample was adjacent to the detector during the count). Each gamma-ray activity considered involved two dominant gamma-ray lines in the spectrum (see Table 3). The

relative yields of these lines were all consistent with the available calibration and decay branching information (within the experimental errors). Appropriate averages of the experimental results (corrected for decay and detector efficiency) were calculated. These average values were used to determine the total number of activated atoms of each type present in the samples.

C. Neutron-Scattering Corrections

The measured fission and sample-activation data had to be corrected for neutron-scattering effects prior to their utilization in cross-section ratio determinations. In essence, this amounted to determination of the factors M_F and M_S which correct for the fissions and activation reactions in the samples that are induced by scattered neutrons. These parameters are explicitly defined in Appendix A. This determination was performed with the aid of the Monte-Carlo neutron-scattering code BESCT2, as discussed in Appendix B and in Ref. 35. Neutron scattering cross-section and emission angular-distribution information required for these calculations was obtained from Ref. 16.

A single-scattering approximation was employed since the experimental configuration (shown schematically in Fig. 1) had a relatively low mass, thereby assuring a priori that the scattering corrections would be small. In this approximation, partial scattering factors could be determined separately, component by component, and then added to produce the overall corrections. Neutrons were considered to be scattered predominantly by three physical components: i) the target assembly, ii) the sample, and iii) the fission chamber. No distinction was made between the two different types of nickel-aluminum samples because they are of rather similar mass and composition (see Table 2). The aluminum content in these samples was neglected for scattering purposes since it amounts to only ~ 2% by weight. These scattering corrections are relatively insensitive to the distance between the target assembly and the sample/fission-chamber configuration. Therefore, calculations were only made for the median distance of ~ 8 cm.

Neutron scattering corrections are very sensitive to reaction threshold, with small corrections for high thresholds generally the rule. Information on the energetics of the reactions considered in the present work appears in Table 5. The results of our multiple-scattering calculations are summarized in Tables 6-8.

From Table 6 it is evident that the additional contributions to sample activation from neutron scattering by the target assembly and by the samples themselves are roughly comparable, while

the effects of neutron scattering from the fission chamber are quite small. The fission chamber is located in the hemisphere behind the sample, and neutrons in the MeV range are far less likely to be back-scattered than forward-scattered (see Fig. 1). On the other hand, the fission-chamber scattering component is comparable to the target and sample components insofar as the production of fission events is concerned. The portions of the fission chamber responsible for producing most of the scattered-neutron fission events are the U-deposit backing plate and the adjacent chamber wall, since they are situated between the U-deposit and the neutron source. An imbalance in the effects of fission-chamber scattering for the samples and for the U-deposit is the factor primarily responsible for producing non-negligible net scattering corrections applicable to the measured ratios. These net corrections are in the range 2.8 - 4.9%. From Table 7 it is evident that elastic scattering is the dominant process of concern here, especially for the high-threshold reactions. Non-elastic neutron emission processes absorb energy, and the softer neutron-emission spectra have less impact for all these threshold-reaction processes than do the harder spectra of elastically-scattered neutrons. Table 8 presents the results required for the present cross-section ratio determinations (see Appendix A). Distinct data point labels are used to identify specific experimental values throughout this report. They are defined in Section III.D.

D. Experimental Cross-Section Ratio Determinations

Sixteen distinct experimental integral cross-section ratios were derived from the measured data. These are ratios to the $^{238}U(n,f)$ reaction. The data-point-number allocations are as follows: $^{7}Li(n,n't)^{4}He$ [Data Point Nos. 1-3], $^{27}A\ell(n,p)^{27}Mg$ [Data Point No. 4], $^{27}A\ell(n,\alpha)^{24}Na$ [Data Point Nos. 5-8], $^{58}Ni(n,p)^{58}Co$ [Data Point Nos. 9-12], and $^{60}Ni(n,p)^{60}Co$ [Data Point Nos. 13-16]. Plural determination of a particular physical quantity under varying conditions offers a test of the consistency of the raw data and of the correction procedures. It usually also leads to a reduction in the error.

The cross-section ratio determinations were achieved using code ACTIVB (Appendix A). Some additional corrections were applied by hand to the $^{7}Li(n,n't)^{4}He$ and $^{27}A\ell(n,\alpha)^{24}Na$ results, but the net effect of these was < 1% for each affected data point. The principle corrections calculated by ACTIVB were those for geometry, neutron absorption and anisotropic neutron emission from the beryllium target. The net effect of these corrections was largest for the high-threshold reactions, and for those measurements where samples were placed close

to the neutron source for irradiation. Neutron-emission anisotropy was primarily responsible for this effect. To show this, ACTIVB calculations were performed for each data point using the proper neutron source representation and also using an isotropic representation. A comparison of the calculated results appears in Table 9. It was previously pointed out in Ref. 11 that neutron-emission anisotropy corrections can be sizable. In that reference it was shown that a needed correction for this effect amounting to ~ 9.4% brings the value of the ratio of $^{63}Cu(n,\alpha)^{60}Co$-to-$^{27}Al(n,\alpha)^{24}Na$ reported by Liskien et al. [13] into good agreement with the corresponding calculated value.

The individually-determined integral cross-section ratios obtained in the present investigation appear in Table 10. What is sought, however, is a single ratio value for each distinct reaction. Therefore it is necessary to combine comparable results in order to obtain the best possible value. From a casual glance it would seem as if some of the individual values in Table 10 are discrepant. We must reserve judgment on this matter, and also defer the process of combining comparable results, until after the topic of experimental errors has been considered.

E. Experimental Errors

A careful examination of all the known sources of experimental error and their correlations is essential for three reasons: i) these uncertainties provide quantitative indication of the reliability of the measured values: ii) covariance information is required in order to properly average comparable experimental results by the method of least-squares (e.g., see Ref. 36), and iii) comparison of measured and corresponding calculated values is meaningless unless all the errors involved are taken into consideration. Table 11 lists the sources of experimental error we have examined and indicates the range of magnitudes encountered for these error components. In this section we consider these errors in greater detail, with particular attention to the matter of correlations. It is not indicated in Table 11 which components are random and which are systematic. This is not an oversight since a particular error may be random, fully systematic or partially correlated, depending on the context in which it is viewed. This will be amply clarified in the following discussion.

The particular U-deposit used in this experiment has been assayed on numerous occasions over the last 15 years since it was fabricated. The reproducibility uncertainty is smaller than the quoted U-deposit calibration error of 2%. The assay process involves a neutron-fission cross-section-ratio measurement of ^{238}U-to-^{235}U using very-well calibrated ^{235}U-enriched deposits (see Ref. 26). The dominant source of

uncertainty is the ^{238}U-to-^{235}U neutron-fission cross-section ratio which enters into the calibration. This error is 100%-correlated for all the data points.

Uncertainties in the sample masses and atomic masses are negligible, but uncertainty does arise from isotopic-abundance and element-constituency considerations for these samples. The sample-atom errors and their correlations are summarized in Table 12.

Errors in determining the fission events arise from several sources which will not be detailed. Table 13 summarizes these errors for present purposes. It is evident that the systematic error is dominant for most of the data points.

The errors in measured sample-count yields are entirely random, and they take into account the fact that several samples were counted more than once for the same activity. These errors are documented in Table 14 according to data-point number.

One source of uncertainty in determining the number of active atoms produced during an irradiation can be attributed directly to the decay half-life. This uncertainty is negligible for the ^{24}Na, ^{58}Co and ^{60}Co determinations, but amounts to 0.3% for tritium and 0.1% for the ^{27}Mg determinations. This error is 100%-correlated between data points corresponding to the same reaction, and is uncorrelated otherwise.

Errors can arise due to limitations in measuring the sample exposure time, the elapsed time between the exposure and a particular count, and the count time itself. These are essentially random errors and they are estimated to be negligible expect for data points associated with the $^{27}Al(n,p)^{27}Mg$ (0.3%) and $^{27}Al(n,\alpha)^{24}Na$ (0.1%) reactions.

Error in calibrating the tritium-counting apparatus stems mainly from uncertainty in the NBS tritiated-water standard (0.6%) and statistics (0.2%). It is 100%-correlated for the $^{7}Li(n,n't)^{4}He$ data points. The uncertainties associated with the calibrations for gamma-ray counting are difficult to assess because several detectors were used and the calibration procedure itself is complex, involving, e.g., standard sources, coincidence counting, geometric corrections and photon-absorption corrections. This matter has been examined rather carefully, but it would be impractical to describe our delibrations in detail in this report. Basically, the uncertainties are attributable to statistics and several systematic errors, e.g, standard calibration sources, geometric parameters and photon-absorption cross sections. Correlations between these uncertainties exist because of the presence of various common factors involved in

the measurements, e.g., detectors, samples, photon-absorption cross sections, etc. Table 15 summarizes the estimated uncertainties and correlations which are applicable to the present investigation.

Generally, the activity-decay branching factors for the reactions considered in this experiment are well known. However, we have included some small errors from this source in our analysis, where applicable. This information appears in Table 16.

We estimate a random uncertainty of 0.5% in determining the loss of tritium activity from lithium during the extraction process. No such error arises for the nickel-aluminum samples.

Uncertainties associated with the irradiation geometry affect the measured ratios as follows: Since the U-deposit and sample occupy a slightly different position, the cross-section results are somewhat sensitive to absolute distance from the neutron source. For the lithium-sample measurements there is additional uncertainty due to the fact that the lithium pellets are encapsulated, and their thicknesses can only be inferred from density considerations rather than by direct measurements. Our estimated uncertainties and their correlations appear in Table 17.

As indicated in Section III.D, the corrections for anisotropic emission of neutrons from the target are calculated using code ACTIVB. We assume that the uncertainty in the net correction is ~ 10% since that is approximately the overall uncertainty associated with specification of the neutron spectrum at angles other than zero degrees [11]. The actual uncertainty in the correction varies from data point to data point owing to the dependence of sensitivity on geometry and reaction threshold but it is impractical to try and take these details into account. Our error estimates are listed in Table 18. We have assumed that these errors are 100%-correlated since they have a common origin.

Errors in the neutron-absorption corrections for the sample and fission chamber are directly linked to neutron-total-cross-section errors for the materials involved. The overall errors in the measured ratios amount to ~ 0.5%. They are 100%-correlated for all data points within the same sample category (i.e, lithium vs. nickel-aluminum) and are uncorrelated otherwise. Likewise, we estimate that the overall errors in the measured ratios due to neutron multiple scattering amount to ~ 0.6%. The correlations are 100% for all data points within the same sample category and ~ 70% between sample categories.

The miscellaneous errors (Item 14, Table 11) correspond to several corrections applied by hand to the integral cross-section ratios, as indicated in Section III.D. There is a 100%-correlated error of 0.3%

applicable to all $^{7}Li(n,n't)^{4}He$ reaction measurements but to no others. Data Point No. 5 has a 0.1% error which affects no other data point. This uncertainty was introduced by an unavoidable interruption of the sample irradiation period for a time duration which is non-negligible by comparison with the decay half life. The miscellaneous errors for all the remaining data points are negligible.

The error information provided in this section, and in Tables 11-18, is all that is needed to calculate the total errors and a master correlation matrix for all the data points. This has been done, according to the method described in Ref. 36, and the results are summarized in Table 19.

F. Experimental Results

The information recorded in Tables 10 and 19 might be considered as the final results of this experiment. However, this material is not particularly useful because what is actually desired is a single integral cross-section ratio for each separate reaction relative to ^{238}U fission. The present section discusses a procedure for generating these values. This method has wide applicability to the field of nuclear data, but it is not widely understood nor particularly well documented elsewhere. The present experiment provides an excellent vehicle for demonstrating how to deal with various problems which arise in applying this method, while at the same time illustrating its power and usefulness. For this reason, we choose to discuss the matter in considerable detail in this report.

The problem of reducing a set of several comparable measured values for a particular physical quantity to a single value is essentially a data-evaluation exercise. The present experiment yields such multiple-valued sets of data which must be thus evaluated, excepting the $^{27}Al(n,p)^{27}Mg$-to-$^{238}U(n,f)$ ratio where only one measured value (Data Point No. 4) is available. The evaluation process, in principle, is straightforward and devoid of ambiguities, provided that the errors and their correlations are available for the experimental quantities to be evaluated. This topic is discussed in another context in Ref. 37. The least-squares computer code AVERG which is described in that document is applicable to the situation which is encountered in the present investigation.

It was pointed out in Ref. 37 that the least-squares method of evaluation yields not only the evaluated "best" values and their errors, but it also tests the consistency of the input data. However, it is well known that the evaluation process breaks down, and anomalous results are generated, whenever the algorithm is applied to seriously inconsistent (discrepant) results. This is not an uncommon occurrence, and it is the

principal reason why data evaluation is partially an art and partially a science. There are differences of opinion on how to deal with the problem of discrepancies. One possible approach is thoroughly discussed in Ref. 37. The problem of inconsistent data also arises in the present investigation. Here, we choose to deal with the problem differently from the way it was generally handled in the work of Ref. 37. The main reason for selecting a different approach is that we are intimately familiar with our own data from the present work whereas Ref. 37 deals with collections of often-poorly-documented results from other authors.

As a first step, we employed code AVERG to evaluate the results summarized in Tables 10 and 19. Each particular type of reaction was analyzed separately rather than simultaneously evaluating all five reaction types involved in this experiment. The $^{27}Al(n,p)^{27}Mg$ reaction was excluded from the process since the single value of Table 10 and its error in Table 19 represent our final results for this particular reaction. The results of our first analysis of the remaining data appear in Table 20. The normalized chi-square parameter tests the data consistency, with any value $\lesssim 1$ indicating good consistency (e.g., see Refs. 36 and 37). On this basis, only the $^{60}Ni(n,p)^{60}Co$ data exhibit scatter consistent with the estimated errors. In the case of $^{27}Al(n,\alpha)^{24}Na$ the inconsistency is so bad that the evaluated result is clearly nonsense, thus demonstrating the above-mentioned principle that the least-squares method breaks down in the face of severe inconsistency.

In simplest terms, inconsistency (a normalized chi-square parameter well in excess of unity) exists whenever scatter in the data to be evaluated exceeds what is indicated as "allowable" by the assumed uncorrelated errors. All else being equal, less scatter is tolerated if the indicated correlations are large. Inconsistency can emerge if the results to be evaluated are truly discrepant, but underestimation of the errors (particularly the random errors) can produce a similar effect. Therefore, in the present situation there are two reasonable approaches for dealing with the problem at hand. These will each be discussed below.

If we presume that our estimation of the errors and their correlations (see Section III.E) is completely reasonable, and that these parameters should not be altered, then only one course of action is available to us in the quest for consistency: We must reject some of the measured values in Table 10 prior to performing the evaluation. A logical procedure for doing this is as follows: First, calculate the impact of each of the available data points on chi-square. Then, reject first the value that will lead to the largest reduction in chi-square. This process should be repeated with remaining data points

if the chi-square still exceeds unity by a significant margin. Once a chi-square near unity is achieved, no more points should be rejected. This approach, which we label "Method 1", is not a reasonable one if chi-square near unity cannot be achieved, or if most of the points end up having to be rejected. We applied Method 1 to the present data and obtained the results indicated in Table 21.

In general, rejection of experimental data is not a desirable method for seeking consistency unless the collection of available data is sufficiently large so that one can be fairly sure from a statistical point of view that certain observed deviations are highly improbable. Rejection is also warranted if specific anomalies which could produce such deviations are discovered in the experiment itself. Neither of these conditions appear to be satisfied in the present situation. Application of the Method 1 evaluation procedure leads to rejection of 25% of the available data from this experiment. Since we found this to be too drastic a step, we sought another evaluation approach which allowed for better use of our data.

A careful check of the measurement procedures, experimental data and the analysis procedures provided no justifications for changing any of the measured values given in Table 10. Therefore, the only remaining recourse was to consider altering our estimates of the errors. The systematic error sources appear to us to be reasonably well substantiated. The only random errors we have quoted are statistical in nature. We therefore decided to assume that the deviations in the measured results which seem to be responsible for the inconsistencies indicated in Table 20 were produced by unknown random effects. Since there is no way of knowing which data points might have been affected, we avoid bias by simply adding equal percentage random errors to all the data points to be evaluated in a particular category, rejecting none of the data points a priori. The amount of added error was that needed to bring the normalized chi-square parameter to the vicinity of unity. We have designated this approach to evaluation as "Method 2". The results of this analysis appear in Table 22. In general, the evaluated results of Method 2 do not differ substantially from those of Method 1, and the errors are not much greater either. Method 2 represents a much more conservative approach than Method 1 because it generally avoids rejection of data. We had to make one exception: the $^{27}Al(n,\alpha)^{24}Na$ reaction. The amount of random error which has to be added to each measured point (20%) in order to be able to retain Data Point No. 7 in the evaluation process seemed excessive based on our judgment with respect to the present experiment. Consequently, we rejected this data point in accordance with Method 1, and then proceded with Method 2. The outcome of this hybrid approach, as well as that from the unaltered application of Method 2, appear in Table 22. Table 23 provides our recommended values for the experimental integral-cross-section ratios from this investigation, as well as their errors and

correlations. The indicated correlations reflect the additional random errors.

It is of interest to consider experimental ratios other than those relative to ^{238}U neutron fission which can be derived from the present results. The information of Table 23 can be used to calculated secondary ratios and their indicated errors, according to a method described in Ref. 36. The results of this analysis are documented in Table 24.

IV. INTEGRAL/DIFFERENTIAL ANALYSIS AND COMPARISONS

The present chapter discusses the methods used to calculate integral reaction cross-section ratios and their uncertainties. Comparisons are also made with the experimental values discussed in Section III.F.

A. Calculated Integral Cross-Section Ratios and Errors

Integral cross sections can be computed from differential-spectrum and cross-section information using Eq. (C.1). For present purposes we have chosen to use the spectrum representation of Crametz et al. [12] and evaluated neutron-induced reaction cross section values from ENDF/B-V [16]. A straightforward numerical integration procedure was employed, with the available tabulated values interpolated as needed for the analysis. This analytical procedure is described in Ref. 38. Knowledge of the spectrum shape for the $^{9}Be(d,n)^{10}B$ thick-target neutron spectrum at 7-MeV deuteron energy is fragmentary below about 1-MeV neutron energy. This clearly impacts upon determination of the absolute integral cross sections for each reaction, however, the ratios of these integral cross sections are little affected for the reactions presently considered. The ratios which were calculated in this fashion are presented in Table 25. Figure 2 indicates the important response ranges of each of the considered reaction cross sections in the present spectrum. From this figure it is clear which portion of the excitation function is tested by the present integral experiment for each reaction.

In order to provide for a meaningful comparison of experimental and calculated integral cross-section ratios, it is necessary to de-

termine uncertainties for the calculated values. The procedure for performing these calculations is described in Appendix C. Group representations were employed for the spectrum and for each of the reaction cross sections. Since the utmost in accuracy was not demanded for these uncertainty calculations, it was decided to utilize a coarse, twelve-group representation for the physical quantities involved. This reduced to a manageable level the volume of input information required for the calculations. The twelve-group representations employed in the present analysis are documented in Tables 26-32. The ratio errors calculated by this method appear in Table 25 along with the calculated ratio values themselves.

B. Comparison of Experimental and Calculated Results

The experimental results from the present investigation are summarized in Tables 23 and 24. They can be compared with the corresponding calculated results of Table 25. These results are also shown in graphical form in Fig. 3.

In this figure, all values are plotted with respect to corresponding experimental quantities. For this reason, the experimental results, which are indicated by solid horizontal bars, are all centered on unity. The bars indicate the errors, e.g., if the bar extends from 0.95 to 1.05, this implies that the experimental result has an error of 5%. In the same fashion, the calculated quantities are indicated by open bars. These have midpoints indicated since their locations are variable. If the midpoint of one of these open bars is located at, e.g., 1.1, this signifies that the ratio of the calculated value to the corresponding experimental one (i.e., C/E) is 1.1. The width of an open bar reflects only the error in the indicated calculated quantity.

Figure 3 clearly demonstrates two general features of the present results:

(1) The errors in the calculated quantities are all larger than those for the corresponding experimental ones. These errors reflect the rather substantial uncertainties assumed for the differential quantities, especially for the ENDF/B-V [16] evaluated cross sections. The magnitude of these errors are indicated in Tables 26-32.

(2) There is excellent agreement between the experimental and calculated values for several integral cross-section ratios of interest

in the present work. In fact, the agreement is far better than is to be expected given the errors involved. Such good agreement is probably largely fortuitious, even in view of the fact that some of the errors may be too large. For the remaining quantities, there seems to be a systematic bias between the experimental and calculated results. On closer inspection, it is seen that there are favorable calculated-to experimental (C/E) comparisons for those reactions having higher thresholds, and thus little response to the present neutron spectrum below around 3 MeV. Similarly, the two reactions with lower thresholds, namely ^{238}U neutron fission and $^{58}Ni(n,p)^{58}Co$ also compare favorably. Inconsistencies arise when comparisons are made between reactions with relatively-low thresholds and those with considerably-higher thresholds. Our speculations regarding this observation appear in Chapter V.

As indicated in Item (1) above, the errors in the calculated quantities do seem to be rather large. This phenomenon was also observed in the work reported in Ref. 14. Some commentary on this point is in order. Referring to Appendix C, it is seen that the ratio errors attributable to each of the reactions cross sections and to the spectrum are separable because no correlations are considered to exist between these parameter sets. It is reasonable to make the assumption that the spectrum errors are unrelated to the cross-section errors, but not that the cross-section errors between reaction type are totally uncorrelated. Unfortunately, the level of development of the ENDF/B-V (Ref. 16) uncertainty files is not well advanced, so there is no alternative to our assumption. Introduction of such reaction-to-reaction correlations would reduce the calculated ratio errors substantially. Furthermore, upon inspection of the work of Crametz et al. (Ref. 12), we are led to suspect that the correlations in the spectrum uncertainties above around 3-4 MeV are underestimated. For most of the spectrum, the overall uncertainty is dominated by the detector efficiency uncertainty, and we feel that this should probably be more strongly correlated than was originally supposed. Increase of the spectrum uncertainty correlations would amount to assuming that the shape of this spectrum is actually better known at the higher-energy range than the numerical representation indicates. Again, this assumption would lower the uncertainties in the calculated quantities.

For the benefit of the reader, we have shown in Table 33 the three independent error components which combine to form the total calculated ratio error for each ratio of interest, as listed in Table 25. It is seen that there are wide variations from ratio to ratio, but generally the magnitudes of the spectrum-related and cross-section-related error contributions are comparable. The spectrum errors have the least impact whenever the two differential cross-section shapes are similar. The spectrum, on the other hand, introduces rather large error whenever one reaction is quite sensitive to the sudden discontinuity in the spectrum near 6 MeV while the other reaction is insensitive to it. Sensitivity to the cross-section excitation function depends upon the

response energy range and also upon whether the cross-section errors are assumed to be strongly correlated. Cross-sections with weakly-correlated errors introduce less ratio error because the integral response averages down the uncertainty. All in all, the importance of the error correlations cannot be overemphasized. It is our belief that the current knowledge of the error correlations for the differential cross-sections from ENDF/B-V (Ref. 16) and for the beryllium spectrum is simply not good enough to permit uncertainties in derived quantities such as the integral response ratios of this work to be estimated with very much reliability. The same outcome is surely to be anticipated in the calculation of even more complex quantities, e.g., the operating parameters of a reactor. In principle, knowledge of covariances for such fundamental quantities as cross sections and neutron spectra is desirable. In practice, there exists a considerable risk of reaching rather misleading conclusions if the knowledge of the uncertainties is imperfect.

V. DISCUSSION OF THE METHOD AND CONCLUSIONS

First, we find that the results of the present investigation imply an excellent degree of consistency between the experimental integral results and the corresponding differential reaction cross-section excitation functions from ENDF/B-V [16]. We indicate below why we suspect that the C/E discrepancies mentioned in Chapter IV are more likely to be caused by problems with the contemporary representation of the thick-target $^{9}Be(d,n)^{10}B$ spectrum rather than with the cross sections which are being subjected to an integral test. As pointed out in Chapter IV, the reactions with higher thresholds demonstrate a considerable degree of internal consistency, as do those two with lower thresholds. Considering that several of these cross sections are rather well-known, it is very unlikely that significant C/E discrepancies could arise due to the cross sections themselves. Thus, we reach the interesting and important conclusion that the $^{7}Li(n,n't)^{4}He$ and $^{60}Ni(n,p)^{60}Co$ cross-section representations given in ENDF/B-V [16] are consistent with experimental observation, at least with respect to the tested response intervals. The differential cross-section evaluation for $^{7}Li(n,n't)^{4}He$ has not been subjected to an experimental verification in the threshold region recently. This energy range, which is tested in the present experiment, is an important one from the point of view of tritium breeding in the blankets of fusion reactors. The $^{60}Ni(n,p)^{60}Co$ reaction is probably of greater importance as a long-lived neutron-fluence dosimeter than it is from a materials-damage point of view. The reaction is of particular importance in the dosimetry context because nickel is a constituent of stainless steel, and is thus continuously present in such important reactor components as the core (for thermal and fast-fission reactors) and the containment vessel (for all types of reactors). Nickel alloys may also be used in the first wall of fusion reactors.

One could bring the calculated integral ratios into better agreement with the measured ones throughout if adjustments were made to the zero-degree thick-target $^{9}Be(d,n)^{10}B$ spectrum representation at neutron energies below ~ 3 MeV, leaving the higher-energy portion of the spectrum as it is represented by the work of Crametz et al. [12]. The number of neutrons present in the low-energy portion of the spectrum (say below ~ 3 MeV) apparently needs to be increased relative to the rest of the spectrum. We have made no attempt here to adjust the spectrum in this fashion. There are very plausible reasons for speculating that the contemporary representation might possibly be in error at lower energies. The spectrum measurements by Crametz et al. [12] were performed using an organic-liquid scintillation detector which had been calibrated several years earlier [39]. The energy region below a few MeV is an especially difficult one, both to calibrate and to reproduce at a later time in such experimental setups. The shape of the calibration curve at higher energies is far less sensitive to the measurement conditions. It would not take much of a discrepancy in reproducing the bias level of the detector to alter the efficiency to an extent which could produce the discrepancies in low-energy response we have observed in this work. In the absence of concrete evidence, this contention is no more than a speculation. A satisfactory resolution of this problem will necessarily involve careful remeasurement of the low-energy portion of the spectrum.

Our investigation supports the conclusion from earlier work (e.g., Refs. 7 and 13) that the thick-target $^{9}Be(d,n)^{10}B$ spectrum can be quite useful for integrally testing activation-reaction cross-section data. Compensating for apparent problems with the low-energy representation of the present spectrum, good C/E consistency was observed for all the reactions considered. The present work has led to a refinement of the methods which are used in such investigations.

The true worth of such integral measurements, since they are somewhat more involved to carryout than monoenergetic studies, lies in assessing what new information could potentially be obtained by performing them. One possible application, namely cross-section unfolding, has been amply discussed in Ref. 9, so we will not repeat the arguments here. Suffice to say, thick target spectra open up the possibility of addressing certain neutron energy regions which otherwise are not easily accessible. Before this application becomes practical, however, it will be necessary to obtain much better knowledge than now exists of neutron-emission spectra for various thick-target reactions at a number of accelerator bombarding energies. This is work for the future. Meanwhile, there appear to be important applications for those spectra which have already been reasonably-well characterized at a few energies, e.g., the $^{9}Be(d,n)^{10}B$ reaction at 7-MeV deuteron energy. One such application is the investigation of very weak activities which cannot be amply produced

using conventional monoenergetic sources. These may involve high-Z elements which have intrinsically-low reaction cross sections, or reactions with long-decay-lifetime products, or exotic charged-particle emission processes.

Is the thick-target $^{9}Be(d,n)^{10}B$ neutron source sufficiently intense, relative to some of the available monoenergetic sources, to make such an avenue of research worth the pursuit? Several years ago we conducted an investigation of the relative intensities of three neutron sources commonly employed in our laboratory. To do this, we employed a fission detector which contained a deposit of uranium enriched in ^{235}U. This provided an essentially flat-response detector which could be used to measure the relative neutron output from these sources. Both proton and deuteron beams were employed, but in each instance the bombarding energy was 7.6 MeV, somewhat above the 7 MeV being considered in the present work. The results of this investigation are reported in Ref. 40. The important conclusions from this earlier study are reproduced in Table 34. It is seen that the thick-target $^{9}Be(d,n)^{10}B$ reaction is a factor of 3000 more intense than the $^{7}Li(p,n)^{7}Be$ reaction and a factor of 257 more intense than the $^{2}H(d,n)^{3}He$ reaction. Figured into these factors are various practical considerations related to target design (e.g., Refs. 41 and 42) as well as to the fundamental cross sections. Sheer intensity of the neutron output is no guarantee that the spectrum will be useful for neutron-reaction investigations. What really counts is the response of the reactions to the spectrum. Thus, we have made a comparison of the relative responses of two reactions, $^{58}Ni(n,p)^{58}Co$ which has a relatively-low threshold and $^{60}Ni(n,p)^{60}Co$ which has a significantly-higher threshold (as per Table 5), in each of the neutron fields under comparison. It is seen in Table 34 that the beryllium spectrum provides a significantly higher reaction yield than the other two sources. Even for the $^{60}Ni(n,p)^{60}Co$ reaction, where the comparison is the least favorable, the thick-target spectrum provides about a factor of 20 more yield than its nearest competitor.

VI. SUMMARY

The following integral reaction rates are measured in the neutron field produced by 7-MeV deuteron bombardment of a thick beryllium metal target: i) reactions with effective thresholds below 3 MeV: $^{238}U(n,f)$ and $^{58}Ni(n,p)^{58}Co$ and ii) reactions with effective thresholds above 3 MeV: $^{7}Li(n,n't)^{4}He$, $^{27}Al(n,p)^{27}Mg$, $^{27}Al(n,\alpha)^{24}Na$ and $^{60}Ni(n,p)^{60}Co$.

Experimental integral cross-section ratios and their uncertainties are deduced using methods described in detail in this report (Tables 23 and 24). It is observed that the analysis is particularly sensitive to anisotropic emission of the neutrons from the target. The measured ratios are compared with corresponding calculated values based on ENDF/B-V differential cross sections (Fig. 3). Uncertainties in the calculated quantities are taken into consideration according to procedures which are also well documented in this report. The present experimental evidence supports the ENDF/B-V differential evaluations for these reactions. It is found that the contemporary covariance information available for the neutron spectrum and for the various differential cross sections most likely leads to an over estimation of uncertainties for the calculated integral cross-section ratios. Also, systematic discrepancies observed in the ratios of low-threshold to high-threshold integral reactions cross sections indicate a deficiency in the zero-degree neutron-spectrum representation for the neutron source which will have to be resolved by further specific investigations of the spectrum.

ACKNOWLEDGEMENTS

The authors are indebted to H. Liskien and J. Van Audenhove of the Central Bureau for Nuclear Measurements, Geel, Belgium, for providing the special nickel-aluminum alloy samples used in this experiment. This work was supported by the U.S. Department of Energy.

APPENDIX A:

Procedure for Deriving Experimental Integral Neutron-Activation Cross-Section Ratios

---

The numerical procedure presently used to calculate integral reaction cross-section ratios from the experimental data bears a resemblance to methods we have reported for other neutron sources, i.e., $^{7}Li(p,n)^{7}Be$ [34], $^{2}H(d,n)^{3}He$ [43], and $^{3}H(d,n)^{4}He$ at low deuteron energy [32]. The essential point is that geometric effects, neutron absorption and multiple-scattering effects, reaction cross-section energy dependence and neutron-source properties must all be taken into account in order to properly determine the relationship between the fundamental processes, the observables, and the experimental arrangement.

The interested reader should refer to Fig. 7 of Ref. 32. This figure defines the significant geometric parameters for the present problem, so we avoid reproducing it in this report. The only difference is that "Be target" should replace "Ti-T Target" for the present application.

In the present work we sought to determine cross-section ratios for sample activation (S) relative to ^{238}U neutron fission (F). Since the neutron-emission spectrum of the beryllium target has only been characterized for neutron energies $\gtrsim$ 1 MeV, our investigation focused entirely on reactions with effective thresholds above ~ 1 MeV. For this reason, a uranium deposit with essentially 100% ^{238}U content was used, thus avoiding difficulties with low-energy fission events.

The spectrum-averaged cross section $\langle\sigma_P\rangle$ for a particular reaction P (P represents either S or F, as indicated above) is given by

$$\langle\sigma_P\rangle = \int_0^\infty \phi(E)\,\sigma_P(E)dE \Big/ \int_0^\infty \phi(E)dE \ , \qquad (A.1)$$

for neutron spectrum $\phi(E)$ and energy differential reaction cross section $\sigma_P(E)$. The denominator term insures proper normalization of the result.

The expression

$$Y_S = G_S \langle\sigma_S\rangle \qquad (A.2)$$

states that the yield Y_S of activated atoms for the sample depends on the spectrum-average cross section and a number of multiplicative factors which are lumped into G_S.

Likewise,

$$Y_F = G_F \langle \sigma_F \rangle \qquad (A.3)$$

relates the measured fissions to the ^{238}U spectrum-averaged fission cross section, with G_F representing the corresponding corrections.

Combining Eqs. (A.2) and (A.3) gives the result

$$R = \langle \sigma_S \rangle / \langle \sigma_F \rangle = (Y_S/Y_F)\ (G_F/G_S) \qquad (A.4)$$

for the integral cross-section ratio R. The fission-reaction energy-differential cross section $\sigma_F(E)$ is assumed to be a known standard over the response range in spectrum $\phi(E)$, thus $\langle \sigma_F \rangle$ can be calculated when $\phi(E)$ is known. Our present concern is with calculation of the factors G_S and G_F.

Knowledge of the spectrum from the target which is limited to zero degrees is inadequate because the samples and uranium deposit (U-deposit) subtend substantial solid angles in typical poor-geometry irradiation environments. The neutron fluence must therefore be mathematically represented by an energy- and angle-dependent function, $\Phi(E,\theta)$. The zero-degree fluence is thus $\Phi(E,0)$. Alternatively, one can write

$$\Phi(E,\theta) = \phi(E)\ S(E,\theta) \quad , \qquad (A.5)$$

with $S(E,0) = 1$. This is a useful approach since $\phi(E)$ is generally specified in more detail than $S(E,\theta)$. For the present work, numerical values representing $\phi(E)$ were obtained from Ref. 12 while those for $S(E,\theta)$ were derived from Ref. 11.

The total fission yield Y_F is the sum of incremental U-deposit fission-yield components Y_{Fij}, namely

$$Y_F = \sum_{ij} Y_{Fij} \quad . \qquad (A.6)$$

The incremental fission yields Y_{Fij} can be calculated using the formula

$$Y_{Fij} = \Phi_{Fij} \ell_{Fj}^{-2} \sigma_{Fi}\ n_F\ V_{Fj}\ \eta_{Fij}\ M_F \quad , \qquad (A.7)$$

where

Φ_{Fij} = neutrons/sr. in energy group "i" emitted in the direction of the U-deposit element with volume V_{Fj},

ℓ_{Fj} = distance from the neutron source (approximated by a point) to the center of the U-deposit element with volume V_{Fj},

η_{Fij} = a neutron absorption factor which is calculated by taking the sample, fission detector and U-deposit backing into consideration,

n_F = ^{238}U atoms/cm^3 of the U-deposit,

σ_{Fi} = differential ^{238}U fission cross section in the vicinity of neutron energy E_i,

M_F = a neutron multiple-scattering correction factor (see Appendix B).

The volume element V_{Fj} is calculated from the formula

$$V_{Fj} = 2\pi R_F^2 X_F (j-1/2)/J^2 \qquad (j=1,J) \ . \tag{A.8}$$

R_F is the U-deposit radius, X_F is its thickness, and J is the selected "mesh" size for the analysis. It is properly assumed that X_F is so small that absorption and geometric effects do not vary across the thickness of the U-deposit.

Now, following the approach represented by Eq. (A.5), we have

$$\Phi_{Fij} = \phi_i \ S_{Fij} \ . \tag{A.9}$$

Furthermore, let d_F be the distance from the neutron source to the center of the U-deposit, then

$$\ell_{Fi}^2 = d_F^2 + r_{Fj}^2 \quad , \tag{A.10}$$

with

$$r_{Fj} = (R_F/J)\ (j - 1/2) \qquad (j=1,J) \ . \tag{A.11}$$

Then Eq. (A.7) can be written in the form

$$Y_{Fij} = \phi_i \ S_{Fij} \ (d_F^2 \ell_{Fj}^{-2}) \sigma_{Fi} n_F V_{Fj} \eta_{Fij} M_F d_F^{-2} \ . \tag{A.12}$$

Now, define

$$C_{Fij} = S_{Fij}(d_F^{2}\ell_{Fj}^{-2})\eta_{Fij} \quad , \tag{A.13}$$

then

$$Y_{Fij} = n_F M_F d_F^{-2}\phi_i \sigma_{Fi} C_{Fij} V_{Fj} \quad . \tag{A.14}$$

If N_F is the total number of ^{238}U atoms in the U-deposit and

$$V_F = \pi R_F^{2} X_F \tag{A.15}$$

is the volume of the U-deposit, then

$$n_F = N_F/V_F \quad , \tag{A.16}$$

so

$$Y_{Fij} = N_F M_F d_F^{-2}(\phi_i \sigma_{Fij} C_{Fij} V_{Fj} V_F^{-1}) \quad . \tag{A.17}$$

Then, from Eq. (A.6) we have

$$Y_F = N_F M_F d_F^{-2} \sum_{ij} \phi_i \sigma_{Fi} C_{Fij} V_{Fj} V_F^{-1} \quad . \tag{A.18}$$

We can split the sum indicated in Eq. (A.18) into two parts by noting that

$$C_{Fij} = 1 + (C_{Fij} - 1) \quad . \tag{A.19}$$

Then

$$Y_F = N_F M_F d_F^{-2} \left[\sum_{ij} \phi_i \sigma_{Fi} V_{Fj} V_F^{-1} + \sum_{ij} \phi_i \sigma_{Fi}(C_{Fij} - 1) V_{Fj} V_F^{-1}\right] \tag{A.20}$$

However,

$$\sum_{ij} \phi_i \sigma_{Fi} V_{Fj} V_F^{-1} = \sum_{i} \phi_i \sigma_{Fi} \left(\sum_{j} V_{Fj} V_F^{-1}\right) = \sum_{i} \phi_i \sigma_{Fi} = \langle \sigma_F \rangle, \tag{A.21}$$

from the definition of $\langle \sigma_F \rangle$ and V_{Fj} .

Therefore,

$$Y_F = N_F M_F d_F^{-2} \left[\langle \sigma_F \rangle + \sum_{ij} \phi_i \sigma_{Fi} (C_{Fij-1}) V_{Fj} V_F^{-1}\right] \tag{A.22}$$

We can easily rewrite Eq. (A.22) in the form

$$Y_F = N_F M_F d_F^{-2} \langle \sigma_F \rangle (1 + \varepsilon_F) \quad , \tag{A.23}$$

where

$$\varepsilon_F = [\sum_{ij} \phi_i \sigma_{Fi} (C_{Fij} - 1) V_{Fj}] V_F^{-1} [\sum_{ij} \phi_i \sigma_{Fi} \delta_{ij}]^{-1} \quad , \tag{A.24}$$

for

$$\delta_{ij} = \begin{cases} 0 & i \neq j \ , \\ 1 & i = j \ . \end{cases} \tag{A.25}$$

This analysis has thus provided an expression for the factor G_F, namely

$$G_F = N_F M_F d_F^{-2} (1 + \varepsilon_F) \quad . \tag{A.26}$$

Calculation of the absorption factors of η_{Fij} is accomplished using the formulas

$$\eta_{Fij} = \exp[(-s_{Si} h_S q_{FSj} - s_{Bi} X_B)/\cos\theta_{Fj}] \quad , \tag{A.27}$$

$$\theta_{Fj} = \tan^{-1} (r_{Fj}/d_f) \quad , \tag{A.28}$$

where

h_S = sample thickness,

q_{FSj} = a factor to handle sample edge effects,

s_{Si} = sample macroscopic total cross section,

s_{Bi} = effective macroscopic cross section for material between the sample and U-deposit,

X_B = thickness of material between the sample and U-deposit.

In an analogous fashion, we have for the sample

$$Y_S = \sum_{ijk} Y_{Sijk} \ . \tag{A.29}$$

Note that the incremental sample activated-atom-yield components involve an additional degree of freedom because geometric and absorption factors can vary significantly across the sample if it is reasonably thick. The expression

$$Y_{Sijk} = \Phi_{Sijk}\, \ell_{Sjk}^{-2}\, \sigma_{Si}\, n_S\, V_{Sjk}\, \eta_{Sijk}\, M_S \qquad (A.30)$$

for the sample is equivalent to Eq. (A.7) for the U-deposit, with

Φ_{Sijk} = neutrons/sr. in energy group "i" emitted in the direction of the sample element with volume V_{Sjk},

ℓ_{Sjk} = distance from the point neutron source to the center of the sample element,

n_S = number of atoms/cm^3 in the sample of the species which contributes to the reaction under consideration,

σ_{Si} = differential reaction cross section in the vicinity of neutron energy E_i,

η_{Sijk} = sample neutron absorption factor,

M_S = the neutron multiple-scattering correction factor (see Appendix B).

We will avoid detailed derivations for the sample since they are quite similar to those for the U-deposit. The results can be obtained using the following formulas:

$$r_{Sj} = (R_S/J)\ (j - 1/2)\ , \qquad (A.31)$$

$$V_{Sijk} = (2\pi\ R_S^2\ h_S/K\ J^2)\ \ (j - 1/2)\ , \qquad (A.32)$$

$$\Phi_{Sijk} = \phi_i\ S_{Sijk}\ , \qquad (A.33)$$

$$L_S = d_N + 1/2\ h_S, \qquad (A.34)$$

$$C_{Sijk} = S_{Sijk}\ L_S^2\ \ell_{Sjk}^{-2}\eta_{Sijk}\ , \qquad (A.35)$$

$$V_S = \sum_{jk} V_{Sjk} = \pi R_S^2 h_S\ , \qquad (A.36)$$

$$N_S = n_S V_S\ , \qquad (A.37)$$

$$X_{Sk} = (h_S/K)\ (k - 1/2)\ , \qquad (A.38)$$

$$\ell_{Sjk}^2 = (d_N + X_{Sk})^2 + r_{Sj}^2\ , \qquad (A.39)$$

$$\theta_{Sjk} = \tan^{-1}\ [r_{Sj}/(d_N + X_{Sk})]\ , \qquad (A.40)$$

$$\eta_{Sjk} = \exp\ (-s_{Si}\ x_{Sk}/\cos\theta_{Sjk})\ , \qquad (A.41)$$

$$Y_S = N_S M_S L_S^{-2}\ \langle\sigma_S\rangle\ (1 + \varepsilon_S)\ , \qquad (A.42)$$

$$\varepsilon_S = \left[\sum_{ijk} \phi_i \sigma_{Si} (C_{Sijk} - 1) V_{Sjk}\right] \left[\sum_{ijk} \phi_i \sigma_{Si} \delta_{ij} \delta_{ik}\right]^{-1} V_S^{-1}$$

$$G_S = N_S M_S L_S^{-2} (1 + \varepsilon_S) \quad . \tag{A.43}$$

The FORTRAN program ACTIVB has been developed to perform this analysis. Energy- and angle-dependent information is introduced in the form of tables which are then linearly interpolated to obtain required numerical values. The most complicated interpolation procedure is that involved in the calculation of $S(E,\theta)$. That procedure is the following:

Tables: $E_1, E_2, \ldots, E_I \quad (i=1,I)$,

$\theta_1, \theta_2, \ldots, \theta_L \quad (\ell=1,L)$,

$S_{i\ell} \; (i = 1,I; \quad \ell=1,L)$.

Given E and θ, find i and ℓ such that

$$E_i \leq E < E_{i+1},$$

$$\theta_\ell \leq \theta < \theta_{\ell+1} \quad .$$

Next, define

$$\alpha = S_{i\ell} + (E-E_i) (S_{i+1,\ell} - S_{i\ell})/(E_{i+1}-E_i) \; , \tag{A.45}$$

$$\beta = S_{i,\ell+1} + (E-E_i) (S_{i+1,\ell+1} - S_{i,\ell+1})/(E_{i+1}-E_i) \quad . \tag{A.46}$$

Then

$$S(E,\theta) \approx \alpha + (\theta-\theta_\ell) (\beta-\alpha) (\theta_{\ell+1}-\theta_\ell)^{-1} \quad . \tag{A.47}$$

ACTIVB can be run on a microcomputer. A listing of the code source appears at the end of this Appendix, along with input and output for a sample problem. For further information contact the authors (DLS).

The input and output parameters of code ACTIVB are defined below. The reader is referred to the source listing and sample problem material for format information:

ACTIVB Input Parameters

(IRD, IWR)

These are program-control parameters which are entered from the computer console (Unit 4).

IRD = Unit number for primary input device, e.g., a card reader.

IWR = Unit number for primary output device, e.g., a printer.

(IC)

This is a flag which indicates the nature of the operations to be executed next by the computer.

IC = 1 Pause and return to control section upon resumption of execution.

IC = 2 A complete set of input data is to be read.

IC = 3 A partial set of input data is to be read, and current values in the computer memory are used for the remaining parameters.

All of the following parameters are read when IC=2:

(N238)

Designates the number of energy (MeV)-cross section (b) pairs for the standard-reaction cross-section table. Presumably a fission reaction is employed. Cross-section values are deduced by linear interpolation of this table.

(E238(I), SIG238(I), I=1, N238).

Energy and cross-section table for the standard reaction.

(NSTM)

Designates the number of energy (MeV)-macroscopic cross-section (cm^{-1}) pairs for the sample total-cross-section table.

(ESTM(I), SIGTM(I), I=1, NSTM)

Energy and macroscopic cross section table for the sample total cross section.

(NSTBM)

Designates the number of energy (MeV)-macroscopic cross-section (cm^{-1}) pairs for backing material located between the sample and uranium deposit.

(ESTBM(I), SIGTBM(I), I=1, NSTBM).

Energy and macroscopic cross section table for sample-backing total cross section.

The two preceding cross section sets are employed in ACTIVB for neutron-absorption calculations. If the absorbers are compounds or have more than one layer (such as the Aℓ-clad Li samples in the present work) this can be handled in part by constructing suitable macroscopic cross section tables.

(NSIGR)

Designates the number of energy (MeV)-cross section (only relative shape vs. energy is required) pairs for the sample-activation cross section.

(ESIGR(I), SIGR(I), I=1, NSIGR)

Energy and cross-section table for the sample-activation cross section. Only the shape is needed, and this does not have to be very well known since it only enters in the evaluation of normally small corrections.

(NPHI)

Number of neutron-energy mesh points in the representation of the zero-degree neutron spectrum $\phi(E)$.

(EPHI(I), PHI(I), I=1, NPHI)

Tabular representation for the zero-degree neutron spectrum.

(NES)

Number of neutron-energy mesh points in the representation of the shape $S(E,\theta)$ of the neutron-emission spectrum

(ES(I), I=1, NES)

Neutron energies associated with the $S(E,\theta)$ table.

(NTHS)

Number of neutron-emission-angle mesh points in the representation of $S(E,\theta)$.

(THS(I), I=1, NTHS)

Neutron-emission angles (in radius) associated with the $S(E,\theta)$ table.

((S(I,J), I=1, NS)J=1, NTHS)

Tabular representation of $S(E,\theta)$.

When IC=3 only the following parameters are read:

(LABEL(I), I=1, 40)

80-column user-selected BCD label for calculational problem.

(NRF,NRS,NHS,NE)

Mesh parameters for ACTIVB calculations.

NRF = radial mesh for uranium deposit.

NRS = radial mesh for sample.

NHS = thickness mesh for sample.

NOTE: The uranium deposit is so thin that it is treated as a single non-absorbing film of negligible thickness.

NE = neutron-energy mesh size employed in the evaluation of the sample and uranium-deposit correction factors.

Development tests of code ACTIVB indicated that the choices NRF=30, NRS=20, NHS=10 and NE=200 provide acceptable accuracy with reasonable computation times. Little is gained by using finer mesh selections. Coarser meshes can be used to speed up the computations, but noticeable sacrifice of accuracy may result.

(ELO,EHI,EMESH)

ELO and EHI are the low and high energies for all calculations performed using the zero-degree neutron emission spectrum $\phi(E)$.

EMESH is a parameter which determines the level of refinement used in calculating $\langle \sigma_F \rangle$. This is not linked with the mesh parameter NE which is involved in other aspects of the ACTIVB analysis. For present purposes, the values ELO=0.1, EHI=12.0 and EMESH=0.1 were found to be suitable.

(RF)

Radius of uranium deposit (cm).

(DF)

Distance from neutron source (a point) to the uranium deposit (cm).

(ATU238)

Absolute number of atoms in the uranium deposit which produce the observed monitor fissions. A single isotope is assumed. In the present work it is ^{238}U.

(YF)

Total observed fissions, corrected for all perturbing effects.

(VMF)

Multiple-scattering correction factor for the fission events.

NOTE: VMF $\geq$ 1 always.

(RS)

Sample radius (cm).

(HS)

Sample thickness (cm).

(DN)

Distance from neutron source to front of the sample (cm).

(ATS)

Absolute number of atoms in the sample which participate in the production of the activity under consideration.

(YS)

Absolute number of atoms activated during the irradiation, corrected for all perturbing effects.

(VMS)

Multiple-scattering correction factor for the sample activations.

NOTE: VMS $\geq$ 1 always.

(XB)

Spacing between sample and uranium deposit (cm).

ACTIVB Output Parameters

Some of the output is a repeat of the input and does not need further definition.

(VLF,VLS)

VLF = DF
VLS = DN + 0.5*HS

(EPSF, EPSS)

Calculated values of ϵ_F (Eq. (A.24)) and ϵ_S (Eq. (A.43)), respectively.

(RATIO, AVSIGF, AVSIGR)

Calculated integral cross section ratio R (Eq. (A.4)), $\langle\sigma_F\rangle$ and $\langle\sigma_S\rangle$, respectively.

ACTIVB Source Listing

```
      PROGRAM ACTIVB
C     ACTIVB - D.L. SMITH - CDC 1700 - X2-6021 (314-109)
C
      COMMON E238(200),SIG238(200),ESTM(200),SIGTM(200),ESTBM(200),SIGTB
     1M(200),ESIGR(200),SIGR(200),LABEL(40),EPHI(200),PHI(200),ES(50),TH
     2S(25),S(50,25)
C
      VALUE(IV,NV,VH,VL)=VL+(VH-VL)*(FLOAT(IV)-0.5)/FLOAT(NV)
      VINT(XL,XH,VL,VH,X)=VL+(X-XL)*(VH-VL)/(XH-XL)
C
C     INITIALIZATION AND CONTROL
C
 1000 WRITE(4,1001)
 1001 FORMAT(/6HACTIVB)
      WRITE(4,1002)
 1002 FORMAT(/11HI/O DEVICES)
      WRITE(4,1003)
 1003 FORMAT(25HINPUT-IRD,WRITE-IWR (2I2)/)
      READ(4,1004) IRD,IWR
 1004 FORMAT(2I2)
    1 READ(IRD,2) IC
    2 FORMAT(I1)
      GO TO(10,20,30),IC
   10 PAUSE
      GO TO 1000
C
C     READ INTERPOLATION TABLES ON UNIT IRD
C
   20 READ(IRD,21) N238
   21 FORMAT(16I5)
      READ(IRD,22) (E238(I),SIG238(I),I=1,N238)
   22 FORMAT(8E10.4)
      READ(IRD,21) NSTM
      READ(IRD,22) (ESTM(I),SIGTM(I),I=1,NSTM)
      READ(IRD,21) NSTBM
      READ(IRD,22) (ESTBM(I),SIGTBM(I),I=1,NSTBM)
      READ(IRD,21) NSIGR
      READ(IRD,22) (ESIGR(I),SIGR(I),I=1,NSIGR)
      READ(IRD,21) NPHI
      READ(IRD,22) (EPHI(I),PHI(I),I=1,NPHI)
      READ(IRD,21) NES
      READ(IRD,22) (ES(I),I=1,NES)
      READ(IRD,21) NTHS
      READ(IRD,22) (THS(I),I=1,NTHS)
      DO 25 J=1,NTHS
   25 READ(IRD,22) (S(I,J),I=1,NES)
```

```
C
C       READ OTHER PARAMETERS ON UNIT IRD
C
   30 READ(IRD,31)  (LABEL(I),I=1,40)
   31 FORMAT(40A2)
      READ(IRD,21)  NRF,NRS,NHS,NE
      READ(IRD,22)  ELO,EHI,EMESH
      READ(IRD,22)  RF,DF,ATU238,YF,VMF
      READ(IRD,22)  RS,HS,DN,ATS,YS,VMS
      READ(IRD,22)  XB
C
C       MISCELLANEOUS
C
      THF1=ATAN(RS/DN)
      THF2=ATAN(RS/(DN+HS))
      VLF=DF
      VLS=DN+0.5*HS
C
C       CALCULATE SPECTRUM AVERAGE CROSS SECTION FOR U-238 MONITOR
C       REACTION IN ZERO-DEG SPECTRUM
C
      SUMNUM=0.0
      SUMDEN=0.0
      EN=ELO
   50 CALL INTRPL(N238,E238,SIG238,EN,VS238,INDEX)
      IF(INDEX.EQ.0) GO TO 10
      CALL INTRPL(NPHI,EPHI,PHI,EN,VPHI,INDEX)
      IF(INDEX.EQ.0) GO TO 10
      SUMNUM=SUMNUM+VS238*VPHI
      SUMDEN=SUMDEN+VPHI
      EN=EN+EMESH
      IF(EN.LT.EHI) GO TO 50
      AVSIGF=SUMNUM/SUMDEN
C
C       CALCULATE FISSION MONITOR CORRECTION FACTOR EPSF
C
      SUMNUM=0.0
      SUMDEN=0.0
      DO 100 I=1,NE
      EN=VALUE(I,NE,EHI,ELO)
      CALL INTRPL(N238,E238,SIG238,EN,VS238,INDEX)
      IF(INDEX.EQ.0) GO TO 10
      CALL INTRPL(NPHI,EPHI,PHI,EN,VPHI,INDEX)
      IF(INDEX.EQ.0) GO TO 10
      CALL INTRPL(NSTM,ESTM,SIGTM,EN,VSTM,INDEX)
      IF(INDEX.EQ.0) GO TO 10
      CALL INTRPL(NSTBM,ESTBM,SIGTBM,EN,VSTBM,INDEX)
      IF(INDEX.EQ.0) GO TO 10
      SUMDEN=SUMDEN+VS238*VPHI
      DO 100 J=1,NRF
      RFJ=VALUE(J,NRF,RF,0.0)
      VLFJ2=RFJ*RFJ+DF*DF
      THFJ=ATAN(RFJ/DF)
      PATHBF=XB/COS(THFJ)
      IF(THFJ.LE.THF2)  PATHSF=HS/COS(THFJ)
      IF(THFJ.GE.THF1)  PATHSF=0.0
      IF(THFJ.GT.THF2.AND.THFJ.LT.THF1)  PATHSF=(RS/SIN(THFJ))-(DN/COS(TH
     1FJ))
```

```
      ATTNF=EXF(-PATHSF*VSTM-PATHBF*VSTBM)
      CALL FINDI(NES,ES,EN,IS,INDEX)
      IF(INDEX.EQ.0) GO TO 10
      CALL FINDI(NTHS,THS,THFJ,LS,INDEX)
      IF(INDEX.EQ.0) GO TO 10
      A=VINT(ES(IS),ES(IS+1),S(IS,LS),S(IS+1,LS),EN)
      B=VINT(ES(IS),ES(IS+1),S(IS,LS+1),S(IS+1,LS+1),EN)
      SFIJ=VINT(THS(LS),THS(LS+1),A,B,THFJ)
      CFIJ=SFIJ*VLF*VLF*ATTNF/VLFJ2
  100 SUMNUM=SUMNUM+VS238*VPHI*(CFIJ-1.0)*FLOAT(2*J-1)/FLOAT(NRF*NRF)
      EPSF=SUMNUM/SUMDEN
C
C     CALCULATE SAMPLE CORRECTION FACTOR EPSS
C
      SUMNUM=0.0
      SUMDEN=0.0
      DO 200 I=1,NE
      EN=VALUE(I,NE,EHI,ELO)
      CALL INTRPL(NSIGR,ESIGR,SIGR,EN,VSIGR,INDEX)
      IF(INDEX.EQ.0) GO TO 10
      CALL INTRPL(NPHI,EPHI,PHI,EN,VPHI,INDEX)
      IF(INDEX.EQ.0) GO TO 10
      CALL INTRPL(NSTM,ESTM,SIGTM,EN,VSTM,INDEX)
      IF(INDEX.EQ.0) GO TO 10
      SUMDEN=SUMDEN+VSIGR*VPHI
      DO 200 J=1,NRS
      RSJ=VALUE(J,NRS,RS,0.0)
      DO 200 K=1,NHS
      XSK=VALUE(K,NHS,HS,0.0)
      VLSJK2=RSJ*RSJ+(DN+XSK)*(DN+XSK)
      THSJK=ATAN(RSJ/(DN+XSK))
      PATHSS=XSK/COS(THSJK)
      ATTNS=EXF(-PATHSS*VSTM)
      CALL FINDI(NES,ES,EN,IS,INDEX)
      IF(INDEX.EQ.0) GO TO 10
      CALL FINDI(NTHS,THS,THSJK,LS,INDEX)
      IF(INDEX.EQ.0) GO TO 10
      A=VINT(ES(IS),ES(IS+1),S(IS,LS),S(IS+1,LS),EN)
      B=VINT(ES(IS),ES(IS+1),S(IS,LS+1),S(IS+1,LS+1),EN)
      SSIJK=VINT(THS(LS),THS(LS+1),A,B,THSJK)
      CSIJK=SSIJK*VLS*VLS*ATTNS/VLSJK2
  200 SUMNUM=SUMNUM+VSIGR*VPHI*(CSIJK-1.0)*FLOAT(2*J-1)/FLOAT(NHS*NRS*NR
     1S)
      EPSS=SUMNUM/SUMDEN
C
C     CALCULATE MEASURED SPECTRUM-AVERAGE CROSS SECTION RATIO AND
C     RESULTANT REACTION SPECTRUM-AVERAGE CROSS SECTION
C
      RATIO=YS*ATU238*VMF*VLS*VLS*(1.0+EPSF)/YF/ATS/VMS/VLF/VLF/(1.0+EPS
     1S)
      AVSIGR=RATIO*AVSIGF
C
C     PRINT NON-TABULAR INPUT AND RESULTS ON UNIT IWR
C
      WRITE(IWR,500)
  500 FORMAT(//5H-----)
      WRITE(IWR,501) (LABEL(I),I=1,40)
  501 FORMAT(//40A2)
```

```
      WRITE(IWR,502) NRF,NRS,NHS,NE
  502 FORMAT(/14HNRF,NRS,NHS,NE/4I5)
      WRITE(IWR,503) ELO,EHI,EMESH
  503 FORMAT(13HELO,EHI,EMESH/3E11.4)
      WRITE(IWR,504) RF,DF,ATU238,YF,VMF
  504 FORMAT(19HRF,DF,ATU238,YF,VMF/5E11.4)
      WRITE(IWR,505) RS,HS,DN,ATS,YS,VMS
  505 FORMAT(19HRS,HS,DN,ATS,YS,VMS/6E11.4)
      WRITE(IWR,506) XB
  506 FORMAT(2HXB/E11.4)
      WRITE(IWR,507) VLF,VLS
  507 FORMAT(7HVLF,VLS/2E11.4)
      WRITE(IWR,508) EPSF,EPSS
  508 FORMAT(9HEPSF,EPSS/2E11.4)
      WRITE(IWR,509) RATIO,AVSIGF,AVSIGR
  509 FORMAT(19HRATIO,AVSIGF,AVSIGR/3E11.4)
C
      GO TO 1
      END
      SUBROUTINE INTRPL(N,XT,YT,X,Y,INDEX)
      DIMENSION XT(2),YT(2)
      INDEX=1
      IF(X-XT(1)) 1,3,4
    1 WRITE(4,2)
    2 FORMAT(8HRANG ERR)
      INDEX=0
      GO TO 24
    3 Y=YT(1)
      GO TO 24
    4 IF(X-XT(N)) 7,5,1
    5 Y=YT(N)
      GO TO 24
    7 I=0
      J=N
    8 K=0.5*FLOAT(J-I)+0.1
      K=K+I
      IF(X-XT(K)) 9,10,11
    9 J=K
      GO TO 12
   10 Y=YT(K)
      GO TO 24
   11 I=K
   12 IF(J-I-1) 13,13,8
   13 I=J
      J=I-1
      DEN=XT(J)-XT(I)
      C1=(XT(J)*YT(I)-XT(I)*YT(J))/DEN
      C2=(YT(J)-YT(I))/DEN
      Y=C1+C2*X
   24 RETURN
      END
      SUBROUTINE FINDI(N,XT,X,IX,INDEX)
      DIMENSION XT(2)
      INDEX=1
      IF(X-XT(1))1,3,4
    1 WRITE(4,2)
    2 FORMAT(8HRANG ERR)
```

```
      INDEX=0
      GO TO 24
    3 IX=1
      GO TO 24
    4 IF(X-XT(N))7,5,1
    5 IX=N-1
    7 I=0
      J=N
    8 K=0.5*FLOAT(J-I)+0.1
      K=K+I
      IF(X-XT(K))9,10,11
    9 J=K
      GO TO 12
   10 IX=K-1
      GO TO 24
   11 I=K
   12 IF(J-I-1)13,13,8
   13 IX=I
   24 RETURN
      END
      FUNCTION EXF(Z)
      IF(Z) 1,1,3
    1 IF(Z.LT.-70.0) Z=-70.0
      IF(Z.GT.-.1E-04) GO TO 2
      EXF=EXP(Z)
      GO TO 4
    3 IF(Z.GT.70.0) Z=70.0
      IF(Z.LT..1E-04) GO TO 2
      EXF=EXP(Z)
      GO TO 4
    2 EXF=1.0+Z
    4 CONTINUE
      RETURN
      END
```

ACTIVB Sample Input

```
2
  110                  U-238(N.F) V
0.0000E-010.2656E-030.1000E-100.2656E-030.2530E-070.5280E-050.1000E-050.8398E-06
0.1000E-050.0000E-010.4000E-020.0000E-010.4000E-020.3000E-040.5000E-020.2500E-04
0.6000E-020.5500E-040.8500E-020.9500E-040.1000E-010.1050E-030.2000E-010.9000E-04
0.4000E-010.6500E-040.8000E-010.5500E-040.1000E-000.6500E-040.3000E+000.1139E-03
0.3500E+000.1862E-030.3800E+000.2342E-030.4000E+000.2527E-030.4200E+000.2773E-03
0.4300E+000.2773E-030.4400E+000.2846E-030.4500E+000.2865E-030.4600E+000.2924E-03
0.4700E+000.3054E-030.5000E+000.3785E-030.5500E+000.6330E-030.5800E+000.6946E-03
0.5900E+000.7630E-030.6000E+000.8271E-030.6200E+000.9328E-030.6400E+000.1134E-02
0.6500E+000.1246E-020.6600E+000.1301E-020.6800E+000.1583E-020.7000E+000.1726E-02
0.7500E+000.2588E-020.7800E+000.3598E-020.8000E+000.4495E-020.8500E+000.7208E-02
0.8800E+000.1083E-010.9000E+000.1370E-010.9200E+000.1558E-010.9500E+000.1663E-01
0.9700E+000.1591E-010.1000E+010.1712E-010.1020E+010.1665E-010.1030E+010.1702E-01
0.1050E+010.1955E-010.1080E+010.2480E-010.1100E+010.2885E-010.1130E+010.3389E-01
0.1140E+010.3564E-010.1150E+010.3763E-010.1170E+010.4047E-010.1200E+010.4332E-01
0.1230E+010.4158E-010.1240E+010.4297E-010.1250E+010.4581E-010.1280E+010.5916E-01
0.1300E+010.7059E-010.1350E+010.1125E+000.1400E+010.1889E+000.1450E+010.2838E+00
0.1480E+010.3299E+000.1500E+010.3467E+000.1550E+010.3802E+000.1600E+010.4063E+00
0.1700E+010.4474E+000.1800E+010.4891E+000.1900E+010.5189E+000.2000E+010.5337E+00
0.2100E+010.5388E+000.2200E+010.5417E+000.2400E+010.5300E+000.2500E+010.5242E+00
0.2800E+010.5312E+000.3000E+010.5226E+000.3100E+010.5228E+000.3500E+010.5327E+00
0.3700E+010.5439E+000.4000E+010.5457E+000.4200E+010.5478E+000.4500E+010.5492E+00
0.5000E+010.5334E+000.5500E+010.5474E+000.6000E+010.6126E+000.6200E+010.6064E+00
0.6400E+010.7736E+000.6500E+010.8091E+000.6600E+010.8398E+000.6800E+010.8935E+00
0.7000E+010.9218E+000.7500E+010.9871E+000.8000E+010.9910E+000.9000E+010.9984E+00
0.1000E+020.9820E+000.1100E+020.9867E+000.1150E+020.9873E+000.1200E+020.9848E+00
0.1300E+020.1020E+010.1350E+020.1067E+010.1400E+020.1120E+010.1450E+020.1172E+01
0.1500E+020.1216E+010.1600E+020.1272E+010.1700E+020.1274E+010.1800E+020.1288E+01
0.1900E+020.1336E+010.2000E+020.1418E+01
```

```
   23
 .0000E 00 .1268E 00 .1000E-05 .4849E-01 .1000E-01 .4826E-01 .1000E 00 .4274E-01
 .2000E 00 .7813E-01 .2500E 00 .4826E 00 .3000E 00 .1241E 00 .4000E 00 .5607E-01
 .5000E 00 .4826E-01 .6000E 00 .4780E-01 .1000E 01 .7124E-01 .1300E 01 .8043E-01
 .2000E 01 .8043E-01 .2500E 01 .8870E-01 .3000E 01 .9422E-01 .3500E 01 .9835E-01
 .4500E 01 .1172E 00 .5500E 01 .9652E-01 .6000E 01 .9881E-01 .7000E 01 .8962E-01
 .8000E 01 .8457E-01 .1500E 02 .6434E-0120.0       0.0386
   24
0.0         0.5794     0.1         0.5794     0.2         0.6881     0.318      0.427
0.428       0.602      0.514       0.5438     0.626       0.4077     0.749      0.5634
0.874       0.515      1.008       0.447      1.123       0.3664     1.248      0.4789
1.349       0.4816     1.46        0.4665     2.01        0.4402     2.5        0.4988
3.0         0.4588     4.0         0.4519     5.0         0.4437     6.04       0.4389
7.05        0.4118     8.05        0.394      14.5        0.3203     20.0       0.25
   72                LI-7(N,N-T)ALPHA V-REV
0.1000E-150.1000E-090.1000E+010.1000E-090.2821E+010.1000E-090.2821E+010.1000E-09
0.2900E+010.7513E-040.3000E+010.2961E-030.3100E+010.6213E-030.3200E+010.1022E-02
0.3300E+010.1533E-020.3400E+010.2091E-020.3500E+010.2221E-020.3600E+010.2247E-02
0.3700E+010.3724E-020.3800E+010.8891E-020.3900E+010.1759E-010.4000E+010.2768E-01
0.4100E+010.3856E-010.4200E+010.4900E-010.4300E+010.5845E-010.4400E+010.6780E-01
0.4500E+010.7719E-010.4600E+010.8624E-010.4700E+010.9295E-010.4800E+010.9824E-01
0.4900E+010.1034E+000.5000E+010.1086E+000.5100E+010.1223E+000.5200E+010.1441E+00
0.5300E+010.1711E+000.5400E+010.2057E+000.5500E+010.2553E+000.5600E+010.3196E+00
0.5700E+010.3399E+000.5800E+010.3504E+000.5900E+010.3575E+000.6000E+010.3624E+00
0.6250E+010.3675E+000.6500E+010.3710E+000.6750E+010.3724E+000.7000E+010.3735E+00
0.7250E+010.3746E+000.7500E+010.3756E+000.7750E+010.3757E+000.8000E+010.3748E+00
0.8250E+010.3733E+000.8500E+010.3717E+000.8750E+010.3699E+000.9000E+010.3681E+00
0.9250E+010.3661E+000.9500E+010.3640E+000.9750E+010.3616E+000.1000E+020.3593E+00
0.1050E+020.3546E+000.1100E+020.3498E+000.1150E+020.3442E+000.1200E+020.3372E+00
0.1250E+020.3290E+000.1300E+020.3208E+000.1350E+020.3125E+000.1400E+020.3042E+00
0.1450E+020.2960E+000.1500E+020.2879E+000.1550E+020.2798E+000.1600E+020.2717E+00
0.1650E+020.2636E+000.1700E+020.2556E+000.1750E+020.2479E+000.1800E+020.2408E+00
0.1850E+020.2342E+000.1900E+020.2279E+000.1950E+020.2218E+000.2000E+020.2159E+00
```

107

0.000001	19.41	1.05	19.41	1.051	19.41	1.15	19.86
1.25	20.44	1.35	20.0	1.45	20.73	1.55	21.54
1.65	21.89	1.75	22.07	1.85	23.10	1.95	23.14
2.05	23.18	2.15	23.47	2.25	23.47	2.35	23.36
2.45	23.45	2.55	23.28	2.65	23.01	2.76	22.86
2.86	22.66	2.96	22.1	3.05	22.4	3.14	22.0
3.24	21.2	3.34	20.86	3.45	20.43	3.55	19.3
3.64	18.68	3.75	18.51	3.87	18.44	3.95	18.33
4.04	18.38	4.14	17.61	4.26	16.85	4.35	16.59
4.46	16.52	4.56	16.08	4.65	15.7	4.73	15.62
4.85	15.51	4.97	15.45	5.04	15.16	5.09	14.64
5.14	14.21	5.19	13.98	5.24	13.32	5.30	12.43
5.35	12.12	5.43	11.88	5.55	11.78	5.63	11.59
5.72	11.67	5.84	11.62	5.94	11.25	6.0	10.84
6.06	9.31	6.13	6.33	6.2	3.99	6.26	3.23
6.33	2.9	6.4	2.68	6.47	2.47	6.55	2.28
6.62	2.12	6.70	2.04	6.81	1.97	6.97	1.98
7.09	1.92	7.17	2.01	7.26	2.03	7.35	2.02
7.43	2.06	7.52	2.16	7.61	2.08	7.71	2.02
7.8	1.89	7.9	1.89	8.0	1.87	8.1	1.92
8.2	1.84	8.3	1.87	8.41	1.91	8.51	1.88
8.62	1.88	8.74	1.85	8.85	1.89	8.97	1.84
9.09	1.79	9.21	1.72	9.33	1.53	9.46	1.43
9.59	1.31	9.72	1.18	9.85	1.08	9.99	1.05
10.13	1.01	10.27	1.0	10.42	0.92	10.56	0.84
10.72	0.75	10.87	0.65	11.03	0.59	11.19	0.58
11.36	0.36	11.4	0.000001	21.0	0.000001		

41

0.0	0.90005	1.10285	1.30985	1.518	1.71835	1.91825	2.121
2.329	2.53505	2.73305	2.94215	3.15995	3.3688	3.5813	3.7934
4.0039	4.2078	4.40325	4.6126	4.83725	5.07875	5.3041	5.51045
5.72905	5.9609	6.2071	6.46885	6.7476	7.04475	7.36195	7.70105
8.06415	8.45355	8.87185	9.322	9.8073	10.3315	10.8989	11.5144
21.0							

```
   21
0.0         0.043633230.087266460.1308997 0.1745329 0.2617994 0.3490659 0.5235988
0.7853982 0.9250245 1.186824  1.308997  1.448623  1.570796  1.745329  1.919862
2.094395  2.268928  2.460914  2.705260  3.1415926
0.1000E+010.1000E+010.1000E+010.1000E+010.1000E+010.1000E+010.1000E+010.1000E+01
0.1000E+010.1000E+010.1000E+010.1000E+010.1000E+010.1000E+010.1000E+010.1000E+01
0.1000E+010.1000E+010.1000E+010.1000E+010.1000E+010.1000E+010.1000E+010.1000E+01
0.1000E+010.1000E+010.1000E+010.1000E+010.1000E+010.1000E+010.1000E+010.1000E+01
0.1000E+010.1000E+010.1000E+010.1000E+010.1000E+010.1000E+010.1000E+010.1000E+01
0.0000E-01
0.1039E+010.1039E+010.1059E+010.1018E+010.1018E+010.1014E+010.1031E+010.1031E+01
0.1025E+010.1025E+010.1021E+010.1023E+010.1016E+010.1039E+010.1021E+010.1021E+01
0.1002E+010.1024E+010.1027E+010.1031E+010.1016E+010.1021E+010.1010E+010.1008E+01
0.1022E+010.1029E+010.1003E+010.1146E+010.1051E+010.1012E+010.1025E+010.1027E+01
0.1069E+010.1066E+010.1120E+010.1138E+010.1111E+010.1185E+010.1200E+010.1234E+01
0.0000E-01
0.9702E+000.9702E+000.1022E+010.9951E+000.9839E+000.9865E+000.9893E+000.9874E+00
0.9809E+000.9776E+000.9817E+000.9867E+000.9734E+000.9820E+000.1001E+010.9800E+00
0.9733E+000.9910E+000.9812E+000.9786E+000.9719E+000.9671E+000.9778E+000.9595E+00
0.9504E+000.9494E+000.1110E+010.1259E+010.1100E+010.1097E+010.1090E+010.1141E+01
0.1189E+010.1163E+010.1231E+010.1317E+010.1433E+010.1419E+010.1526E+010.1975E+01
0.0000E-01
0.9254E+000.9254E+000.9781E+000.9755E+000.9517E+000.9510E+000.9637E+000.9662E+00
0.9474E+000.9452E+000.9479E+000.9448E+000.9291E+000.9300E+000.9253E+000.9273E+00
0.9199E+000.9268E+000.9243E+000.9158E+000.9223E+000.8789E+000.8877E+000.8691E+00
0.8722E+000.8344E+000.6918E+000.1106E+010.1150E+010.1206E+010.1276E+010.1294E+01
0.1412E+010.1442E+010.1535E+010.1551E+010.1695E+010.1862E+010.1696E+010.1164E+01
0.0000E-01
0.9403E+000.9403E+000.9461E+000.9267E+000.9149E+000.8982E+000.8845E+000.8822E+00
0.8707E+000.8674E+000.8572E+000.8507E+000.8419E+000.8400E+000.8500E+000.8379E+00
0.8424E+000.8464E+000.8390E+000.8320E+000.8329E+000.8183E+000.7895E+000.7440E+00
0.7530E+000.7732E+000.9159E+000.1212E+010.1232E+010.1268E+010.1298E+010.1368E+01
0.1486E+010.1526E+010.1686E+010.1868E+010.2131E+010.2250E+010.2336E+010.2956E+01
0.0000E-01
0.8735E+000.8735E+000.8980E+000.8545E+000.8200E+000.7980E+000.7943E+000.7686E+00
0.7546E+000.7444E+000.7325E+000.7206E+000.7033E+000.7001E+000.6922E+000.6974E+00
0.6919E+000.6972E+000.6973E+000.6754E+000.6625E+000.6234E+000.5704E+000.5641E+00
0.5593E+000.5556E+000.6360E+000.1291E+010.1435E+010.1503E+010.1592E+010.1703E+01
0.1967E+010.2055E+010.2257E+010.2455E+010.2925E+010.3172E+010.2974E+010.3004E+01
0.0000E-01
```

0.8259E+000.8259E+000.7899E+000.7482E+000.7308E+000.6992E+000.6611E+000.6441E+00
0.6122E+000.5860E+000.5711E+000.5636E+000.5370E+000.5346E+000.5279E+000.5331E+00
0.5290E+000.5190E+000.5328E+000.5009E+000.5078E+000.4440E+000.3782E+000.3896E+00
0.3969E+000.4045E+000.5202E+000.1341E+010.1582E+010.1687E+010.1787E+010.1853E+01
0.2127E+010.2250E+010.2413E+010.2606E+010.3082E+010.3350E+010.2859E+010.2342E+01
0.0000E-01
0.7071E+000.7071E+000.6570E+000.5853E+000.5372E+000.5051E+000.4745E+000.4485E+00
0.4156E+000.3986E+000.3898E+000.3740E+000.3577E+000.3528E+000.3552E+000.3554E+00
0.3454E+000.3489E+000.3294E+000.3030E+000.3004E+000.2397E+000.2301E+000.2650E+00
0.2799E+000.2745E+000.4521E+000.1252E+010.1522E+010.1593E+010.1659E+010.1695E+01
0.1991E+010.1980E+010.2064E+010.2194E+010.2566E+010.2599E+010.2164E+010.1452E+01
0.0000E-01
0.5312E+000.5312E+000.4807E+000.4246E+000.3939E+000.3551E+000.3308E+000.3086E+00
0.2854E+000.2800E+000.2628E+000.2505E+000.2395E+000.2327E+000.2402E+000.2312E+00
0.2169E+000.1974E+000.1930E+000.1829E+000.1652E+000.1618E+000.1872E+000.2013E+00
0.1778E+000.1844E+000.3265E+000.8903E+000.1067E+010.1041E+010.9177E+000.8939E+00
0.9615E+000.8469E+000.7258E+000.6926E+000.7795E+000.5808E+000.2912E+000.6266E-01
0.0000E-01
0.4712E+000.4712E+000.4245E+000.3764E+000.3581E+000.3158E+000.2992E+000.2791E+00
0.2639E+000.2506E+000.2332E+000.2238E+000.2075E+000.2039E+000.1999E+000.1923E+00
0.1718E+000.1682E+000.1612E+000.1415E+000.1432E+000.1510E+000.1616E+000.1477E+00
0.1413E+000.1563E+000.2876E+000.7548E+000.8523E+000.7237E+000.6532E+000.6129E+00
0.6159E+000.4434E+000.4065E+000.4266E+000.3902E+000.2143E+000.2758E-010.3902E-01
0.0000E-01
0.3575E+000.3575E+000.3586E+000.3305E+000.2958E+000.2717E+000.2491E+000.2326E+00
0.2144E+000.1960E+000.1803E+000.1704E+000.1639E+000.1592E+000.1514E+000.1387E+00
0.1299E+000.1156E+000.1097E+000.1105E+000.1193E+000.1083E+000.1097E+000.1107E+00
0.1146E+000.1274E+000.2209E+000.5524E+000.5350E+000.4871E+000.4547E+000.4141E+00
0.3919E+000.3402E+000.3272E+000.2921E+000.2091E+000.3364E-010.0000E-010.0000E-01
0.0000E-01
0.3290E+000.3290E+000.3333E+000.3094E+000.2729E+000.2480E+000.2289E+000.2088E+00
0.1905E+000.1743E+000.1633E+000.1536E+000.1441E+000.1370E+000.1285E+000.1256E+00
0.1062E+000.9740E-010.1032E+000.1075E+000.1064E+000.9513E-010.9530E-010.1093E+00
0.1134E+000.1188E+000.1983E+000.4728E+000.4884E+000.4657E+000.4150E+000.3847E+00
0.3644E+000.3147E+000.2725E+000.2000E+000.8046E-010.2000E-020.0000E-010.0000E-01
0.0000E-01
0.3059E+000.3059E+000.3179E+000.2883E+000.2623E+000.2278E+000.2155E+000.1911E+00
0.1755E+000.1616E+000.1534E+000.1419E+000.1339E+000.1238E+000.1206E+000.1065E+00
0.9132E-010.9932E-010.1032E+000.1021E+000.1013E+000.8891E-010.9769E-010.1112E+00
0.1115E+000.1147E+000.1771E+000.4540E+000.4880E+000.4388E+000.3940E+000.3435E+00
0.3436E+000.2962E+000.2263E+000.1398E+000.2985E-010.3857E-020.0000E-010.0000E-01
0.0000E-01

0. 3031E+000. 3031E+000. 3107E+000. 2766E+000. 2396E+000. 2166E+000. 1932E+000. 1804E+00
0. 1577E+000. 1515E+000. 1439E+000. 1335E+000. 1187E+000. 1146E+000. 1004E+000. 9048E-01
0. 9023E-010. 9631E-010. 9680E-010. 9188E-010. 8323E-010. 8401E-010. 1031E+000. 1123E+00
0. 1084E+000. 1023E+000. 1708E+000. 4189E+000. 4726E+000. 4388E+000. 3736E+000. 3205E+00
0. 3175E+000. 2314E+000. 1591E+000. 3658E-010. 0000E-010. 0000E-010. 0000E-010. 0000E-01
0. 0000E-01
0. 2707E+000. 2707E+000. 2766E+000. 2455E+000. 2135E+000. 1869E+000. 1708E+000. 1553E+00
0. 1445E+000. 1347E+000. 1230E+000. 1120E+000. 1026E+000. 8953E-010. 7936E-010. 8271E-01
0. 8459E-010. 8473E-010. 8224E-010. 7897E-010. 8460E-010. 8903E-010. 1009E+000. 1088E+00
0. 9272E-010. 9660E-010. 1662E+000. 4206E+000. 4526E+000. 3757E+000. 3141E+000. 3066E+00
0. 2709E+000. 1843E+000. 5766E-010. 2251E-020. 0000E-010. 0000E-010. 0000E-010. 0000E-01
0. 0000E-01
0. 2539E+000. 2539E+000. 2691E+000. 2268E+000. 2004E+000. 1686E+000. 1559E+000. 1419E+00
0. 1285E+000. 1199E+000. 1120E+000. 1001E+000. 8824E-010. 7175E-010. 7489E-010. 8019E-01
0. 7413E-010. 6925E-010. 7134E-010. 8329E-010. 8863E-010. 9643E-010. 1032E+000. 1049E+00
0. 1032E+000. 1008E+000. 1639E+000. 3925E+000. 3852E+000. 3653E+000. 3126E+000. 2777E+00
0. 2439E+000. 1067E+000. 6821E-020. 0000E-010. 0000E-010. 0000E-010. 0000E-010. 0000E-01
0. 0000E-01
0. 2499E+000. 2499E+000. 2549E+000. 2103E+000. 1805E+000. 1604E+000. 1419E+000. 1306E+00
0. 1153E+000. 1068E+000. 9760E-010. 8974E-010. 6952E-010. 6616E-010. 7004E-010. 6948E-01
0. 6406E-010. 6075E-010. 7666E-010. 8493E-010. 9588E-010. 9513E-010. 1024E+000. 1070E+00
0. 1021E+000. 1008E+000. 1668E+000. 3677E+000. 3898E+000. 3752E+000. 3308E+000. 2939E+00
0. 2067E+000. 3281E-010. 6307E-020. 1829E-020. 0000E-010. 0000E-010. 0000E-010. 0000E-01
0. 0000E-01
0. 2345E+000. 2345E+000. 2423E+000. 1945E+000. 1753E+000. 1451E+000. 1342E+000. 1218E+00
0. 1047E+000. 9558E-010. 9325E-010. 7204E-010. 6313E-010. 6255E-010. 6111E-010. 6043E-01
0. 5377E-010. 7070E-010. 8518E-010. 8978E-010. 9757E-010. 9530E-010. 1025E+000. 1082E+00
0. 9755E-010. 9717E-010. 1431E+000. 3803E+000. 4263E+000. 3949E+000. 3057E+000. 2263E+00
0. 4242E-010. 3860E-020. 0000E-010. 0000E-010. 0000E-010. 0000E-010. 0000E-010. 0000E-01
0. 0000E-01
0. 2268E+000. 2268E+000. 2128E+000. 1824E+000. 1591E+000. 1297E+000. 1152E+000. 1072E+00
0. 9387E-010. 8551E-010. 7860E-010. 6130E-010. 5718E-010. 5169E-010. 5277E-010. 5420E-01
0. 5427E-010. 6947E-010. 8161E-010. 9062E-010. 8847E-010. 9048E-010. 9757E-010. 1053E+00
0. 1017E+000. 9450E-010. 1563E+000. 4042E+000. 4520E+000. 3877E+000. 2900E+000. 1560E+00
0. 3648E-010. 1055E-010. 5148E-020. 2110E-020. 0000E-010. 0000E-010. 0000E-010. 0000E-01
0. 0000E-01
0. 2106E+000. 2106E+000. 2134E+000. 1746E+000. 1500E+000. 1264E+000. 1086E+000. 9827E-01
0. 8965E-010. 8339E-010. 6818E-010. 5946E-010. 5447E-010. 4755E-010. 5507E-010. 5479E-01
0. 6450E-010. 8062E-010. 8607E-010. 8575E-010. 9025E-010. 8749E-010. 1025E+000. 1065E+00
0. 9532E-010. 1028E+000. 1756E+000. 4226E+000. 4308E+000. 2852E+000. 1421E+000. 1124E-01
0. 4242E-020. 0000E-010. 0000E-010. 0000E-010. 0000E-010. 0000E-010. 0000E-010. 0000E-01
0. 0000E-01

```
0.2106E+000.2106E+000.2134E+000.1746E+000.1500E+000.1264E+000.1086E+000.9827E-01
0.8965E-010.8339E-010.6818E-010.5946E-010.5447E-010.4755E-010.5507E-010.5479E-01
0.6450E-010.8062E-010.8607E-010.8575E-010.9025E-010.8749E-010.1025E+000.1065E+00
0.9532E-010.1028E+000.1756E+000.4226E+000.4308E+000.2852E+000.1421E+000.1124E-01
0.4242E-020.0000E-010.0000E-010.0000E-010.0000E-010.0000E-010.0000E-010.0000E-01
0.0000E-01
R2199,LI7-1,8CM     DATA POINT 1
   30    20    10   200
0.1          12.0         0.1
1.27         8.226        +.5009E+191.0          1.0
0.959        0.4594       7.666        +.6044E+231.0          1.0
0.0508
3
R2200,LI7-4,8CM     DATA POINT 2
   30    20    10   200
0.1          12.0         0.1
1.27         8.226        +.5009E+191.0          1.0
0.959        0.6316       7.493        +.8308E+231.0          1.0
0.0508
3
R2202,LI7-11,6CM    DATA POINT 3
   30    20    10   200
0.1          12.0         0.1
1.27         6.11         +.5009E+191.0          1.0
0.959        0.6106       5.398        +.8031E+231.0          1.0
0.0508
1
```

ACTIVB Sample Output

```
-----

R2199.LI7-1,8CM     DATA POINT 1

NRF,NRS,NHS,NE
    30    20    10   200
ELO,EHI,EMESH
 0.1000E-00 0.1200E+02 0.1000E-00
RF,DF,ATU238,YF,VMF
 0.1270E+01 0.8226E+01 0.5009E+19 0.1000E+01 0.1000E+01
RS,HS,DN,ATS,YS,VMS
 0.9590E+00 0.4594E+00 0.7666E+01 0.6044E+23 0.1000E+01 0.1000E+01
XB
 0.5080E-01
VLF,VLS
 0.8226E+01 0.7896E+01
EPSF,EPSS
-0.5594E-01 0.3023E-01
RATIO,AVSIGF,AVSIGR
 0.6997E-04 0.4437E+00 0.3105E-04

-----

R2200.LI7-4.8CM     DATA POINT 2

NRF,NRS,NHS,NE
    30    20    10   200
ELO,EHI,EMESH
 0.1000E-00 0.1200E+02 0.1000E-00
RF,DF,ATU238,YF,VMF
 0.1270E+01 0.8226E+01 0.5009E+19 0.1000E+01 0.1000E+01
RS,HS.DN,ATS,YS,VMS
 0.9590E+00 0.6316E+00 0.7493E+01 0.8308E+23 0.1000E+01 0.1000E+01
XB
 0.5080E-01
VLF,VLS
 0.8226E+01 0.7809E+01
EPSF,EPSS
-0.6625E-01 0.2298E-01
RATIO,AVSIGF,AVSIGR
 0.4959E-04 0.4437E+00 0.2200E-04
```

R2202.LI7-11.6CM DATA POINT 3

NRF,NRS,NHS,NE
  30 20 10 200
ELO,EHI,EMESH
 0.1000E-00 0.1200E+02 0.1000E-00
RF,DF,ATU238,YF,VMF
 0.1270E+01 0.6110E+01 0.5009E+19 0.1000E+01 0.1000E+01
RS,HS,DN,ATS,YS,VMS
 0.9590E+00 0.6106E+00 0.5398E+01 0.8031E+23 0.1000E+01 0.1000E+01
XB
 0.5080E-01
VLF,VLS
 0.6110E+01 0.5703E+01
EPSF,EPSS
-0.9677E-01 0.2473E-01
RATIO,AVSIGF,AVSIGR
 0.4790E-04 0.4437E+00 0.2125E-04

APPENDIX B:

Procedure for Deriving Neutron-Scattering Corrections

The corrections for neutron scattering from low-mass target and detector assemblies having coaxial-cylinder geometries were computed using BESCT2, a modification of the Monte-Carlo program CYSCAT which is described in Ref. 35. CYSCAT was designed for monoenergetic sources, and the source weight and energy were calculated from the kinematics of the neutron-producing reaction using information that was part of the input for the problem. BESCT2 is adapted to broad-spectrum sources such as the thick-target neutron yield from the $^{9}Be(d,n)^{10}B$ reaction, but it is essentially the same as CYSCAT except for the source term. The source weight is entered as a two-parameter table giving the emission probability P in terms of $\cos\theta$ and E_n (see Refs. 11 and 12). The table is renormalized at the time of entry so that

$$\iint P(\cos\theta,E_n)d(\cos\theta)dE_n=1. \qquad (B.1)$$

The laboratory angle, as $\cos\theta$, and the neutron energy, E_n, are chosen at random and the source weight is generated from the table using linear interpolation.

Both CYSCAT and BESCT2 are written in FORTRAN and they can be run on a microcomputer. For further information contact the authors (JWM).

APPENDIX C:

Procedure for Deriving Errors in Calculated Integral Neutron-Activation Cross-Section Ratios

---

Procedures for calculating an integral cross section,

$$G = \int_0^\infty \phi(E)\,\sigma(E)dE \qquad \left(\int_0^\infty \phi(E)dE=1\right) \quad , \tag{C.1}$$

and determining the response range ($\phi\sigma$ non-negligible) have been discussed by many authors. In the present work we resort to the method described in Ref. 38, and employ code SENSY.

For two reactions, one has

$$G_i = \int_0^\infty \phi(E)\,\sigma_i(E)dE \qquad (i=1,2) \quad , \tag{C.2}$$

and one can consider the ratio

$$R = G_2/G_1 \quad . \tag{C.3}$$

In the present work we have measured ratios, R, with a certain experimental accuracy. In order to meaningfully compare a measured ratio with one calculated using Eqs. (C.2)-(C.3), one should be in position to also predict an error for the calculated result. This issue is addressed in Ref. 14. Here we outline the formalism used in the present work.

Eq. (C.2) can be approximated by a finite sum,

$$G_i \approx \sum_{k=1}^{n} \phi_k \sigma_{ik} \qquad (i=1,2) \quad . \tag{C.4}$$

The values $\vec{\phi} = (\phi_1,\phi_2,\ldots,\phi_n)$ and $\vec{\sigma}_i = (\sigma_{i1},\sigma_{i2},\ldots,\sigma_{in})$ are group values. In matrix notation, Eq. (C.4) becomes

$$G_i = \vec{\phi} \cdot \vec{\sigma} \quad . \tag{C.5}$$

R can be expressed as a function of several variables, namely

$$R = R(\vec{\sigma}_1, \vec{\sigma}_2, \vec{\phi}) = (\vec{\phi} \cdot \vec{\sigma}_2)/(\vec{\phi} \cdot \vec{\sigma}_1) \quad . \tag{C.6}$$

Now let $\vec{x}$ be defined by

$$\vec{x} = \begin{bmatrix} \vec{\sigma}_1 \\ \vec{\sigma}_2 \\ \vec{\phi} \end{bmatrix} \tag{C.7}$$

Individual components of $\vec{\sigma}_1$, $\vec{\sigma}_2$, and $\vec{\phi}$ all have errors. We designate these by $\vec{E}_{\sigma 1}$, $\vec{E}_{\sigma 2}$ and $\vec{E}_{\phi}$. Thus,

$$\vec{E}_x = \begin{bmatrix} \vec{E}_{\sigma 1} \\ \vec{E}_{\sigma 2} \\ \vec{E}_{\phi} \end{bmatrix} . \tag{C.8}$$

We assume that the errors for $\vec{\sigma}_1$, $\vec{\sigma}_2$ and $\vec{\phi}$ are only correlated within each class, but not between different classes. Thus the correlation matrix for $\vec{x}$ is

$$\overline{C}_x = \begin{bmatrix} \overline{C}_{\sigma_1} & & 0 \\ & \overline{C}_{\sigma_2} & \\ 0 & & \overline{C}_{\phi} \end{bmatrix} \tag{C.9}$$

According to Ref. 36, the error E_R in the ratio R is derived using straightforward error-propagation rules. The applicable formulas are:

$$E_R^2 = (\overline{S} \cdot \vec{E}_x)^T \cdot \overline{C}_x \cdot (\overline{S} \cdot \vec{E}_x) \quad , \tag{C.10}$$

$$\bar{S} = \begin{bmatrix} \partial R/\partial x_1 & & 0 \\ & \ddots & \\ 0 & & \partial R/\partial x_m \end{bmatrix} = \begin{bmatrix} \bar{S}_{\sigma_1} & & 0 \\ & \bar{S}_{\sigma_2} & \\ 0 & & \bar{S}_{\phi} \end{bmatrix} \tag{C.11}$$

$$\bar{S}_{\sigma_i} = \begin{bmatrix} \partial R/\partial \sigma_{i1} & & 0 \\ & \ddots & \\ 0 & & \partial R/\partial \sigma_{in} \end{bmatrix} \quad (i=1,2) \quad , \tag{C.12}$$

$$\bar{S}_{\phi} = \begin{bmatrix} \partial R/\partial \phi_1 & & 0 \\ & \ddots & \\ 0 & & \partial R/\partial \phi_n \end{bmatrix} . \tag{C.13}$$

Note that "T" designates a transposed matrix while m=3n in the preceding equations.

We could also write Eq. (C.10) in the form

$$E_R{}^2 = \sum_{i=1}^{2} (\bar{S}_{\sigma_i} \cdot \vec{E}_{\sigma_i})^T \cdot \bar{C}_{\sigma_i} \cdot (\bar{S}_{\sigma_i} \cdot \vec{E}_{\sigma_i}) \tag{C.14}$$

$$+ (\bar{S}_{\phi} \cdot \vec{E}_{\phi})^T \cdot \bar{C}_{\phi} \cdot (\bar{S}_{\phi} \cdot \vec{E}_{\phi})$$

The partial derivatives in Eqs. (C.12) - (C.13) are calculated using the formulas

$$(\partial R/\partial \sigma_{1k}) = (-G_2/G_1{}^2)\,(\partial G_1/\partial \sigma_{1k})$$

$$= (-G_2/G_1{}^2)\phi_k \qquad (k=1,n) \quad , \tag{C.15}$$

$$(\partial R/\partial \sigma_{2k}) = (1/G_1)\,(\partial G_2/\partial \sigma_{2k})$$

$$= (1/G_1)\phi_k \qquad (k=1,n) \quad , \tag{C.16}$$

$$
\begin{aligned}
(\partial R/\partial \phi_k) &= (1/G_1)\,(\partial G_2/\partial \phi_k) + (-G_2/G_1{}^2)\,(\partial G_1/\partial \phi_k) \\
&= (1/G_1)\,\sigma_{2k} + (-G_2/G_1{}^2)\,\sigma_{1k} \\
&= (G_1\,\sigma_{2k} - G_2\,\sigma_{1k})/G_1{}^2 \qquad (k=1,n) \quad .
\end{aligned}
\tag{C.17}
$$

These calculations are performed using a microcomputer. Input information required includes group cross-section values for the two reactions involved and for the spectrum, as well as their corresponding covariance matrices. For further information contact the authors (DLS).

REFERENCES

1. K. A. Weaver, "Neutrons from Deuteron Bombardment of Light Nuclei", UCRL-51310, Lawrence Livermore Laboratory (1972); see also K. A. Weaver, "Spectra of Neutrons from Deuteron Bombardment of Light Nuclei", UCLR-51310-Addendum, Lawrence Livermore Laboratory (1973).

2. K. A. Weaver, J. D. Anderson, H. H. Barschall, and J. C. Davis, Nuclear Science and Engineering 52, 35 (1973).

3. P. Grand and A. N. Goland, Nuclear Instruments and Methods 145 (1977) 49.

4. M. J. Saltmarsh, C. A. Ludemann, C. B. Fulmer, and R. C. Styles, Nuclear Instruments and Methods 145 (1977) 81.

5. M. A. Lone and B. C. Robertson, "Low Energy Neutron Emission From Be(d,n) and Be(p,n) Reactions", Proceedings of a Symposium on Neutron Cross Sections from 10 to 50 MeV, Brookhaven National Laboratory, Upton, New York, May 12-14, 1980, BNL-NCS-51245 (Vol. I) edited by M. R. Bhat and S. Pearlstein, Brookhaven National Laboratory, July 1980, p. 147.

6. M. A. Lone and C. B. Bingham, "Intense Deuteron and Proton Induced (CW)-Neutron Sources", Neutron Sources for Basic Physics and Applications, edited by S. Cierjacks, Pergamon Press, Oxford, United Kingdom (1983) p. 133.

7. L. R. Greenwood, R. R. Heinrich, R. J. Kennerly, and R. Medrzychowski, Nuclear Technology 41, 109 (1978).

8. L. R. Greenwood and R. R. Heinrich, Journal of Nuclear Materials 85 and 86 (1979) 473.

9. Donald L. Smith, "A Least-Squares Method for Deriving Reaction Differential Cross Section Information from Measurements Performed in Diverse Fields", ANL/NDM-77, Argonne National Laboratory (1982).

10. E. T. Cheng, D. R. Mathews and K. R. Schultz, "Magnetic Fusion Energy Program Nuclear Data Needs", GA-A17754, GA Technologies (1984).

11. D. L. Smith, J. W. Meadows and P. T. Guenther, "Fast-Neutron Spectrum Measurements for the Thick-Target $^{9}Be(d,n)^{10}B$ Reaction at E_d = 7 MeV", ANL/NDM-90, Argonne National Laboratory (1985).

12. A. Crametz, H.-H. Knitter and D. L. Smith, "Thick-Target $^{9}Be(d,n)^{10}B$ Neutron Spectrum at E_d = 7 MeV", Nuclear Data for Science and Technology, edited by K. H. Böckhoff, D. Reidel Publishing Company, Dordrecht, Holland (1983), p. 902.

13. H. Liskien, D. L. Smith, and R. Widera, "The Spectrum-Average Cross Section Ratio of $^{63}Cu(n,\alpha)^{60}Co$-to-$^{27}Al(n,\alpha)^{24}Na$ in a Thick-Target $^{9}Be(d,n)^{10}B$ Neutron Spectrum", Nuclear Data for Science and Technology, edited by K. H. Böckhoff, D. Reidel Publishing Company, Dordrecht, Holland (1983), p. 409.

14. D. L. Smith and H. Liskien, "Error Analysis for the Calculated Spectrum-Average Cross Section Ratio of $^{63}Cu(n,\alpha)^{60}Co$-to-$^{27}Al(n,\alpha)^{24}Na$ in a Thick-Target $^{9}Be(d,n)^{10}B$ Spectrum", European Applied Research Reports, Vol. 4, No. 4, 969-1014 (1982).

15. W. Poenitz, E. Pennington, A. B. Smith and R. Howerton, "Evaluated Fast Neutron Cross Sections of Uranium-238", ANL/NDM-32, Argonne National Laboratory (1977).

16. "Evaluated Neutron Data File, ENDF/B-V", ENDF/B Summary Documentation, compiled by R. Kinsey, ENDF-201, 3rd Edition, Brookhaven National Laboratory (1979).

17. S. A. Cox and P. R. Hanley, IEEE Transactions on Nuclear Science NS-18, No. 3, 108 (1971).

18. E. H. Beckner, R. L. Bramblett, G. C. Phillips and T. A. Eastwood, Physical Review 123, 2100 (1961).

19. Jagdish K. Tuli, "Nuclear Wallet Cards", National Nuclear Data Center, Brookhaven National Laboratory, Upton, NY 11973, USA (1985).

20. H. H. Anderson and J. F. Ziegler, Hydrogen Stopping Powers and Ranges in All Elements, Pergamon Press, New York (1977).

21. Stable Isotopes Division, Oak Ridge National Laboratory, Oak Ridge, Tennessee 37830.

22. Donald L. Smith, Manuel M. Bretscher and James W. Meadows, Nucl. Sci. Eng. 78, 359 (1981).

23. Eastman Kodak Corp., Chemicals Division, Rochester, New York, USA.

24. J. W. Meadows, Nucl. Sci. Eng. 49, 310 (1972).

25. Donald L. Smith and James W. Meadows, "Response of Several Threshold Reactions in Reference Fission Neutron Fields", ANL/NDM-13, Argonne National Laboratory (1975).

26. W. P. Poenitz, J. W. Meadows and R. J. Armani, "^{235}U Fission Mass and Counting Comparison and Standardization", ANL/NDM-48, Argonne National Laboratory (1979).

27. M. M. Bretscher and D. L. Smith, "Thermal Neutron Calibration of a Tritium Extraction Facility Using the $^{6}Li(n,t)^{4}He/^{197}Au(n,\gamma)^{198}Au$ Cross Section Ratio for Standardization", ANL/NDM-55, Argonne National Laboratory (1981).

28. M. M. Bretscher, "Li-6 as a Reference Absorber for Capture-to-Fission Ratio Measurements in Zero Power Fast Critical Assemblies", Reactor Physics Division Annual Report, July 1, 1967 to June 30, 1968, ANL-7410, pp. 178-182, Argonne National Laboratory (1969).

29. M. M. Bretscher, B. M. Oliver and Harry Farrar IV, "Calibrations of a Tritium Extraction Facility", paper presented at the 10th Symposium on Fusion Engineering, Philadelphia, Pennsylvania, December 5-9, 1983. Proceedings are available in book and microfiche form from IEEE Service Center, Single Publication Sales Department, 445 Hoes Lane, Piscataway, New Jersey 08854.

30. Model 2660 Packard Tri-Carb Liquid Scintillation Counter: Packard Instrument Co., Inc., 2200 Warrenville Road, Downers Grove, Illinois 60515.

31. M. P. Unterweger, B. M. Coursey, F. J. Schima and W. B. Mann "Preparation and Calibration of the 1978 National Bureau of Standards Tritiated Water Standards", Int. J. Appl. Rad. and Isotopes 31, 611 (1980). See also A Handbook of Radioactivity Measurements Procedures, NCRP Report No. 58, p. 322 (1978).

32. Donald L. Smith, James W. Meadows, Manuel M. Bretscher and Samson A. Cox, "Cross-Section Measurement for the $^{7}Li(n,n't)^{4}He$ Reaction at 14.74 MeV", ANL/NDM-87, Argonne National Laboratory (1984).

33. James W. Meadows and Donald L. Smith, "Gamma-Ray Detector Calibration Methods Utilized in the Argonne FNG Group Activation Cross Section Measurement Program", ANL/NDM-60, Argonne National Laboratory (1984).

34. Donald L. Smith and James W. Meadows, "Measurement of $^{58}Ni(n,p)^{58}Co$ Reaction Cross Sections for E_n=0.44-5.87 MeV using Activation Methods", ANL-7989, Argonne National Laboratory (1973).

35. D. L. Smith and J. W. Meadows, "Neutron Inelastic Scattering Studies for Lead-204", ANL/NDM-37, Argonne National Laboratory (1977).

36. Donald L. Smith, "Covariance Matrices and Applications to the Field of Nuclear Data", ANL/NDM-62, Argonne National Laboratory (1981).

37. Bernard P. Evain, Donald L. Smith and Paul Lucchese, "Compilation and Evaluation of 14-MeV Neutron Activation Cross Sections for Nuclear Technology Applications: Set I", ANL/NDM-89, Argonne National Laboratory (1985).

38. Donald L. Smith, "Analysis of the Sensitivity of Spectrum-Average Cross Sections to Individual Characteristics of Differential Excitation Functions", ANL/NDM-30, Argonne National Laboratory (1977).

39. H.-H Knitter, A. Paulsen, H. Liskien and M. M. Islam, "Measurements of the Neutron Energy Spectrum of the Spontaneous Fission of ^{252}Cf", Atomkernenergie (ATKE) Bd. 22, Lfg. 2, p. 84 (1973).

40. James W. Meadows and Donald L. Smith, "Neutron Source Investigations in Support of the Cross Section Program at the Argonne Fast-Neutron Generator", ANL/NDM-53, Argonne National Laboratory (1980).

41. J. W. Meadows and D. L. Smith, "Neutrons from Proton Bombardment of Natural Lithium", ANL-7938, Argonne National Laboratory (1972).

42. James W. Meadows, Donald L. Smith and Gerhard Winkler, "A High-Current Deuterium Gas Target for Neutron Nuclear Data Research", Nuclear Instruments and Methods 176, 439 (1980).

43. D. L. Smith and J. W. Meadows, "Method of Neutron Activation Cross Section Measurement for E_n=5.5-10 MeV Using the D(d,n)He-3 Reaction as a Neutron Source", ANL/NDM-9, Argonne National Laboratory (1974).

44. C. M. Lederer et al., Table of the Isotopes, Seventh Edition, John Wiley and Sons, New York (1978).

45. P. M. Endt and C. Van der Leun, Nuclear Physics A310, 1 (1978).

46. L. K. Peker, Nuclear Data Sheets 42, 457 (1984).

47. R. L. Auble, Nuclear Data Sheets 28, 103 (1979).

Table 1: Lithium Sample Properties

Sample	Diameter[a] (cm)	Thickness[a] (cm)	Total[b] Mass (g)	Aℓ Capsule Mass (g)	Lithium Mass (g)	^{6}Li Content (atoms)	^{7}Li Content (atoms)
^{7}Li No. 1[c]	1.918	0.4594	2.5834	1.8786	0.7048	Negligible[f]	6.0440(22)[e] (± 0.1%)
^{7}Li No. 4[c]	1.918	0.6316	2.8153	1.8465	0.9688	Negligible	8.3079(22) (± 0.1%)
^{7}Li No. 11[c]	1.918	0.6106	2.8008	1.8643	0.9365	Negligible	8.30309(22) (± 0.1%)
^{7}Li No. 15[d]	1.918	0.5898	2.7052	1.8966	0.8085	Negligible	8.01968(22) (± 0.1%)

[a]Dimensions of lithium wafer, excluding the encapsulation material.
[b]Lithium plus aluminum capsule.
[c]Irradiated sample.
[d]Unirradiated sample.
[e]6.0440(22) signifies 6.0440×10^{22}.
[f]Impact of the ^{6}Li content on the present experiment is considered to be negligible.

Table 2: Nickel-Aluminum Sample Properties

Sample	Diameter (cm)	Thickness (cm)	Total Mass (g)	Isotope Content (atoms)[a]		
				^{27}Al	^{58}Ni	^{60}Ni
ANL Ni-Al Sandwich	1.905	0.2286	4.722 ± 0.001[c]	2.6607(21)[b] (± 0.5%)	3.2251(22) (± 0.2%)	1.2324(22) (± 0.2%)
CBNM Ni-Al No. 1	2.000 ± 0.002	0.200 + 0.003 - 0.000	5.492 ± 0.001	2.4517(21) (± 1%)	3.7715(22) (± 0.2%)	1.4413(22) (± 0.2%)
CBNM Ni-Al No. 2	2.000 ± 0.002	0.200 + 0.003 - 0.000	5.422 ± 0.001	2.4205(21) (± 1%)	3.7235(22) (± 0.2%)	1.4229(22) (± 0.2%)
CBNM Ni-Al No. 3	2.000 ± 0.002	0.200 ± 0.001	5.404 ± 0.001	2.4125(21) (± 1%)	3.7111(22) (± 0.2%)	1.4182(22) (± 0.2%)
CBNM Ni-Al No. 4	2.000 ± 0.002	0.200 + 0.003 - 0.000	5.443 ± 0.001	2.4299(21) (± 1%)	3.7379(22) (± 0.2%)	1.4284(22) (± 0.2%)

[a]Based on isotopic abundances from Ref. 19. Only those isotopes of nickel which are of concern in the present investigation are shown.

[b]2.6607(21) signifies 2.6607×10^{21}.

[c]Includes 0.093 g attributed to the adhesive material.

Table 3: Reaction-Product Decay Properties

Isotope	Half Life		Decay[a] Modes		Dominant Decay Gamma Rays[b]	
^{3}H	12.35 ± 0.04 y	c	β^-(100%)	d	-	
^{27}Mg	9.458 ± 0.012 m	e	β^-(100%)	e	0.844 MeV (71.8 ± 0.4%) 1.014 MeV (28.2 ± 0.4%)	e e
^{24}Na	15.020 ± 0.007 h	e	β^-(100%)	e	1.369 (100%) Negligible error 2.754 (100%) Negligible error	e e
^{24m}Na (E_x=0.472 MeV)	20.18 ± 0.10 ms	e	IT(~ 100%) β^-($\leq 3 \times 10^{-2}$%)	e e	-	
^{58}Co	70.82 ± 0.03 d	f	ε(~ 85%) β^+(~ 15%)	f	0.811 (100.0 ± 0.3%) 0.511 (30%) annih. rad. Negligible error	f
^{58m}Co (E_x=0.025 MeV)	9.15 ± 0.010 h	f	IT(100%)	f	-	
^{60}Co	5.271 ± 0.001 y	g	β^-(100%)	g	1.173 (99.90 ± 0.02%) 1.333 (99.9824 ± 0.0005%)	g g
^{60m}Co (E_x=0.059 MeV)	10.47 ± 0.04 m	g	IT(99.75 ± 0.03%) β^-(0.25 ± 0.03%)	g g	-	

[a](...) indicates decay-mode branch factor.
[b]Gamma-ray energies in MeV. (...) indicates gamma yield per decay.
[c]Ref. 32.
[d]Ref. 44.
[e]Ref. 45.
[f]Ref. 46.
[g]Ref. 47.

Table 4: Parameters Required for Determination of Lithium-Sample Tritium Content

Sample	Lithium[a] Mass (g)	m(C)/m(E)[b]	Disintegtations of tritium[c] per sec per gram of Lithium
^{7}Li No. 1	0.7048	1.020	30.622 (± 1.5%)
^{7}Li No. 4	0.9688	1.013	37.625 (± 0.4%)
^{7}Li No. 11	0.9365	1.011	29.828 (± 0.3%)

[a]Reproduced from Table 1.

[b]m(C) = calculated mass of extracted water. m(E) = measured mass of extracted water. Ratio is thus a correction factor for hydrogen (and presumably tritium) lost in the extraction process.

[c]Corrected for counting system background, tritium decay half-life and losses in the extraction process. Error is only the random error; it does not include uncertainties in the efficiency determination, tritium half-life or NBS tritiated-water standard calibration.

Table 5: Reaction Energetics[a]

Reaction	Q-Value (MeV)	Threshold Energy (MeV) Theoretical[b]	Effective[c]
^{7}Li(n,n't)^{4}He	-2.468	2.823	~ 3.5
^{27}Aℓ(n,p)^{27}Mg	-1.829	1.897	~ 3
^{27}Aℓ(n,α)^{24}Na	-3.132	3.249	~ 5
^{58}Ni(n,p)^{58}Co	+0.401	-	~ 1
^{60}Ni(n,p)^{60}Co	-2.042	2.076	~ 4
^{238}U(n,f)	-	-	~ 1

[a]Based on data from Ref. 19.

[b]Based on Q-value.

[c]Response $\phi\sigma$ for the 7-MeV ^{9}Be(d,n)^{10}B thick-target spectrum becomes very small below this energy (see Fig. 2).

Table 6: Summary of Neutron-Multiple-Scattering Corrections According to Scatterer[a]

Reaction	Scatterer	Total Scattering[b] Correction (%)
$^{7}Li(n,n't)^{4}He$	Target Assembly	1.6
	Fission Chamber	0.2
	Li Sample	2.0
$^{27}Al(n,p)^{27}Mg$	Target Assembly	1.9
	Fission Chamber	0.3
	Ni-Al Sample	2.5
$^{27}Al(n,\alpha)^{24}Na$	Target Assembly	1.8
	Fission Chamber	0.1
	Ni-Al Sample	2.2
$^{58}Ni(n,p)^{58}Co$	Target Assembly	1.8
	Fission Chamber	0.6
	Ni-Al Sample	3.0
$^{60}Ni(n,p)^{60}Co$	Target Assembly	1.8
	Fission Chamber	0.2
	Ni-Al Sample	2.4
$^{238}U(n,f)$	Target Assembly	2.4
	Fission Chamber	2.7
	Li Sample	3.5
	Ni-Al Sample	3.2

[a]Scattering correction is the ratio of events produced by scattered neutrons to those produced by direct neutrons.

[b]Includes both elastic and non-elastic neutron scattering processes.

Table 7: Summary of Neutron-Multiple-Scattering Corrections According to Process[a]

Reaction	Elastic-Scattering Correction (%)	Non-elastic-Scattering[b] Correction (%)
$^{238}U(n,f)$ (Li sample)	7.0	1.7
$^{238}U(n,f)$ (Ni-Aℓ sample)	6.4	1.9
$^{7}Li(n,n't)^{4}He$	3.6	0.2
$^{27}Aℓ(n,p)^{27}Mg$	4.3	0.3
$^{27}Aℓ(n,\alpha)^{24}Na$	4.0	0.1
$^{58}Ni(n,p)^{58}Co$	4.6	0.9
$^{60}Ni(n,p)^{60}Co$	4.2	0.2

[a]Scattering correction is the ratio of events produced by scattered neutrons to those produced by direct neutrons.

[b]Non-elastic neutron scattering includes all open-channel neutron-emission reactions which are not elastic, e.g., (n,n') and (n,2n).

Table 8: Summary of Neutron-Multiple-Scattering-Corrections According to Application in Cross-Section Ratio Determinations

Data[a] Point No.	Reaction[b]	M_F-1[c] (%)	M_S-1[c] (%)
1-3	$^{7}Li(n,n't)^{4}He$	8.7	3.8
4	$^{27}Aℓ(n,p)^{27}Mg$	8.3	4.6
5-8	$^{27}Aℓ(n,\alpha)^{24}Na$	8.3	4.1
9-12	$^{58}Ni(n,p)^{58}Co$	8.3	5.5
13-16	$^{60}Ni(n,p)^{60}Co$	8.3	4.3

[a]Identifies distinct experimental values from the present work as described in Section III.D.

[b]The ^{238}U neutron-fission reaction serves as the monitor in this experiment so it is not indicated as a particular application.

[c]The factors M_F and M_S are defined in Appendix A.

Table 9: Effect of Neutron-Emission Anisotropy on Integral Cross-Section Ratios Deduced from the Experimental Data.

Reaction[a]	Nominal Sample[b] Distance (cm)	Anisotropy Correction Factor[c]
$^{7}Li(n,n't)^{4}He$	6	1.087
$^{7}Li(n,n't)^{4}He$	8	1.055
$^{27}Al(n,p)^{27}Mg$	8	1.084
$^{27}Al(n,\alpha)^{24}Na$	6	1.475
$^{27}Al(n,\alpha)^{24}Na$	8	1.281
$^{27}Al(n,\alpha)^{24}Na$	10	1.205
$^{58}Ni(n,p)^{58}Co$	6	1.020
$^{58}Ni(n,p)^{58}Co$	8	1.014
$^{58}Ni(n,p)^{58}Co$	10	1.010
$^{60}Ni(n,p)^{60}Co$	6	1.280
$^{60}Ni(n,p)^{60}Co$	8	1.167
$^{60}Ni(n,p)^{60}Co$	10	1.122

[a]The ratio of interest is that of the indicated reaction relative to ^{238}U neutron fission.

[b]Approximate distance from point neutron source to the sample.

[c]If the neutron emission were assumed to be isotropic, then the calculated cross-section ratio would be too large. The correct ratio could be obtained by dividing the result obtained assuming isotropy by the indicated factor.

Table 10: Measured Integral Cross-Section Ratios

Data[a] Point No.	Sample[b]	Reaction[c]	Nominal Sample[d] Distance (cm)	Integral Cross[c] Section Ratio
1	^{7}Li No. 1	^{7}Li(n,n't)^{4}He	8	0.1151
2	^{7}Li No. 4	^{7}Li(n,n't)^{4}He	8	0.1257
3	^{7}Li No. 11	^{7}Li(n,n't)^{4}He	6	0.1262
4	CBNM Ni-Aℓ No. 1	^{27}Aℓ(n,p)^{27}Mg	8	0.02380
5	ANL Ni-Aℓ Sandwich	^{27}Aℓ(n,α)^{24}Na	8	0.005909
6	CBNM Ni-Aℓ No. 2	^{27}Aℓ(n,α)^{24}Na	8	0.006657
7[e]	CBNM Ni-Aℓ No. 3	^{27}Aℓ(n,α)^{24}Na	6	0.004316
8	CBNM Ni-Aℓ No. 4	^{27}Aℓ(n,α)^{24}Na	10	0.006059
9	ANL/Ni-Aℓ Sandwich	^{58}Ni(n,p)^{58}Co	8	0.5377
10	CBNM Ni-Aℓ No. 2	^{58}Ni(n,p)^{58}Co	8	0.5306
11	CBNM Ni-Aℓ No. 3	^{58}Ni(n,p)^{58}Co	6	0.5335
12	CBNM Ni-Aℓ No. 4	^{58}Ni(n,p)^{58}Co	10	0.5190
13	ANL Ni-Aℓ Sandwich	^{60}Ni(n,p)^{60}Co	8	0.01789
14	CBNM Ni-Aℓ No. 2	^{60}Ni(n,p)^{60}Co	8	0.01774
15	CBNM Ni-Aℓ No. 3	^{60}Ni(n,p)^{60}Co	6	0.01751
16	CBNM Ni-Aℓ No. 4	^{60}Ni(n,p)^{60}Co	10	0.01717

[a]Identifies distinct experimental values from the present work as discussed in Section III.D.

[b]See Tables 1 and 2.

[c]The ratio of interest is that of the indicated reaction relative to ^{238}U neutron fission.

[d]Approximate distance from point neutron source to the sample.

[e]Data point rejected due to inconsistency with comparable values. See discussion in Section III.F.

Table 11: Sources of Experimental Error in the Measured Cross-Section Ratios

	Error Source[a]	Magnitude (%)
1.	Number of U-deposit atoms	2.0
2.	Number of sample atoms	0.1 - 1.0
3.	Measured fission events	0.8 - 1.3
4.	Measured sample-count yield	0.3 - 3.0
5.	Activity-decay half life	N[b] - 0.3
6.	Exposure, wait and count times	N - 0.3
7.	Counting-apparatus calibration	0.6 - 3.1
8.	Decay branching	N - 1.0
9.	Activity loss from the sample	N - 0.5
10.	Irradiation geometry	N - 1.7
11.	Neutron-source anisotropy	0.1 - 4.7
12.	Neutron absorption	0.5
13.	Neutron multiple scattering	0.6
14.	Miscellaneous effects	N - 0.3

[a]Details are discussed in Section III.E.
[b]N = negligible.

Table 12: Sample-Atom Errors and Correlations

Group	Data Point Nos.	Isotope	Error (%)[a]	Correlation Matrix[b] 1	2	3	4	5	6	7	8
1	1-3	^{7}Li	0.1	1							
2	4	^{27}Al	1.0	0	1						
3	5	^{27}Al	0.1	0	0	1					
4	6-8	^{27}Al	1.0	0	1	0	1				
5	9	^{58}Ni	0.1	0	0	0	0	1			
6	10-12	^{58}Ni	0.1	0	0	0	0	0	1		
7	13	^{60}Ni	0.1	0	0	0	0	0	0	1	
8	14-16	^{60}Ni	0.1	0	0	0	0	0	0	0	1

[a]Errors are 100%-correlated within each data-point group.
[b]Correlations indicated are those between different data-point groups.

Table 13: Errors in Measured Fission Events

Data Point Nos.	Random Error (%)	Systematic[a] Error (%)	Total[b] Error (%)
6,10,14	0.3	0.7	0.8
1	0.3	0.7	0.8
2	0.3	0.7	0.8
7,11,15	1.1	0.7	1.3
3	1.1	0.7	1.3
5,9,13	0.3	0.7	0.8
4	0.3	0.7	0.8
8,12,16	0.3	0.7	0.8

[a]100%-correlated for all the data points.
[b]100%-correlated within a particular data-point group.

Table 14: Random Errors in Measured Sample-Count Yields

Data Point Nos.	Error (%)	Data Point No.	Error (%)	Data Point No.	Error (%)
1	1.5	7	1.0	13	2.5
2	0.4	8	0.5	14	1.3
3	0.3	9	0.5	15	2.5
4	1.5	10	0.3	16	2.0
5	3.0	11	0.3		
6	0.4	12	0.5		

Table 15: Counting-Apparatus Calibration Errors and Correlations

Group	Data Points Nos.	Activity	Error(%)[a]	Correlation Matrix[b] 1	2	3	4	5
1	1-3	^{3}H	0.6	1				
2	4	^{27}Mg	2.3	0	1			
3	5-8	^{24}Na	3.1	0	.68	1		
4	9-12	^{58}Co	2.3	0	.91	.68	1	
5	13-16	^{60}Co	2.3	0	.46	.21	.28	1

[a]Errors are 100%-correlated within each data-point group.
[b]Correlations indicated are those between different data-point groups.

Table 16: Activity Decay-Branching Errors

Data Point Nos.	Activity	Measured Radiation	Error (%)[a]
1-3	^{3}H	β^-	N[b]
4	^{27}Mg	γ	1.0
5-8	^{24}Na	γ	N
9-12	^{58}Co	γ	0.3
13-16	^{60}Co	γ	N

[a]100%-correlated within a particular data-point group. Uncorrelated otherwise.
[b]N = negligible.

Table 17: Irradiation-Geometry Errors

Data Point Nos.	Error (%)[a]	Data Point Nos.	Error (%)[a]
1	1.3	7,11,15	0.1
2	1.3	6,10,14	0.1
3	1.7	8,12,16	N[b]
5,9,13	0.1		

[a]100%-correlated within a particular data-point group. Uncorrelated otherwise.
[b]N=negligible.

Table 18: Uncertainties Due to Neutron-Source Anisotropy

Data Point No.	Error(%)[a]	Data Point No.	Error (%)[a]
1	0.6	9	0.2
2	0.6	10	0.1
3	0.9	11	0.2
4	0.8	12	0.1
5	2.7	13	1.6
6	2.9	14	1.7
7	4.7	15	2.8
8	2.1	16	1.2

[a]Errors are 100%-correlated for every data point.

Table 19: Errors and Correlations for Measured Integral Cross-Section Ratios[a]

Data Point No.	Total Error (%)	Correlation Matrix															
		1	2	3	4	5	6	7	8	9	10	11	12	13	14	15	16
1	3.2	1															
2	2.9	.65	1														
3	3.3	.59	.65	1													
4	3.9	.42	.46	.42	1												
5	5.6	.36	.39	.39	.55	1											
6	4.9	.41	.46	.45	.69	.82	1										
7	6.3	.38	.41	.43	.60	.78	.95	1									
8	4.5	.42	.46	.45	.72	.81	.99	.90	1								
9	3.3	.46	.51	.45	.78	.58	.65	.52	.70	1							
10	3.3	.45	.50	.44	.78	.55	.64	.50	.68	.96	1						
11	3.4	.45	.49	.44	.76	.55	.63	.56	.68	.94	.94	1					
12	3.3	.45	.50	.44	.78	.55	.63	.50	.69	.96	.96	.94	1				
13	4.4	.40	.45	.43	.51	.45	.52	.51	.50	.49	.46	.46	.46	1			
14	3.9	.46	.51	.49	.58	.51	.61	.59	.58	.54	.54	.52	.52	.76	1		
15	5.1	.39	.43	.43	.49	.50	.59	.65	.54	.42	.41	.48	.41	.66	.76	1	
16	4.0	.43	.47	.44	.54	.44	.51	.49	.51	.52	.51	.50	.52	.70	.80	.67	1

[a]The information provided here supplements the results of Table 10.

Table 20: Straightforward Evaluation of the Present Experimental Integral Cross-Section-Ratio Data Using Code AVERG[a]

Evaluated Data Point Nos.	Reaction	Evaluated[b] Ratio	Error in Evaluated Ratio (%)	Normalized Chi-Square	Consistency
1,2,3	$^{7}Li(n,n't)^{4}He$	0.1214	2.7	7.16	Poor
5,6,7,8	$^{27}A\ell(n,\alpha)^{24}Na$	0.6758(-3)[c]	8.4	169.1	Terrible
9,10,11,12	$^{58}Ni(n,p)^{58}Co$	0.5208	3.3	5.06	Poor
13,14,15,16	$^{60}Ni(n,p)^{60}Co$	0.01750	3.7	0.75	Very Good

[a]Values from Tables 10 and 19 (except for Data Point No. 4) are included in the analysis without alterations.

[b]Ratios are relative to ^{238}U neutron fission.

[c]0.6758(-3) signifies 0.6758×10^{-3}.

Table 21: "Method 1" Evaluation of the Present Experimental Integral Cross-Section-Ratio Data Using Code AVERG[a]

Evaluated Data[b] Point Nos.	Reaction	Evaluated[c] Ratio	Error in Evaluated Ratio (%)	Normalized Chi-Square
[1],2,3	$^{7}Li(n,n't)^{4}He$	0.1259	2.8	0.02
5,[6],[7],8	$^{27}Al(n,\alpha)^{24}Na$	0.006054	4.5	0.60
9,10,11,[12]	$^{58}Ni(n,p)^{58}Co$	0.5329	3.3	1.02
13,14,15,16[d]	$^{60}Ni(n,p)^{60}Co$	0.01750	3.7	0.75

[a]All values from Tables 10 and 19 (except for Data Point No. 4) were considered in the analysis without alterations.

[b]Data points indicated by [...] had to be rejected in order to obtain the evaluated results presented in this table.

[c]Ratios are relative to ^{238}U neutron fission.

[d]No data points were rejected for this reaction, as discussed in Section III.F.

Table 22: "Method 2" Evaluation of the Present Experimental Integral Cross-Section-Ratio Data Using Code AVERG[a]

Evaluated Data[b] Point Nos.	Reaction	Added[c] Random Error (%)	Evaluated Ratio	Error in Evaluated Ratio (%)	Normalized Chi-Square	Comment on Added Random Error
1,2,3	$^{7}Li(n,n't)^{4}He$	5.0	0.1217	4.0	0.96	Reasonable
5,6,7,8	$^{27}Al(n,\alpha)^{24}Na$	20.0	0.005406	11.4	0.97	Excessive
5,6,[7],8	$^{27}Al(n,\alpha)^{24}Na$	6.0	0.006155	5.9	0.98	Reasonable
9,10,11,12	$^{58}Ni(n,p)^{58}Co$	5.0	0.5298	4.1	0.92	Reasonable
13,14,15,16	$^{60}Ni(n,p)^{60}Co$	None[e]	0.01750	3.7	0.75	-

[a]Values from Table 10 (except for Data Point No. 4) were considered in the analysis without alteration.

[b]Data points indicated by [...] had to be rejected in order to obtain the evaluated results presented in this table.

[c]The indicated random error was added to the errors from Table 19 for each evaluated data point.

[d]Ratios are relative to ^{238}U neutron fission.

[e]The measured data for this reaction were consistent with the errors of Table 19. No additional random error was included.

Table 23: Final Primary Experimental Integral Cross-Section Ratios from the Present Investigation[a]

Index	Reaction	Ratio[b]	Ratio Error(%)	Correlation Matrix 1	2	3	4	5
1	$^{7}Li(n,n't)^{4}He$	0.1217	4.0	1				
2	$^{27}Al(n,p)^{27}Mg$	0.02380	3.9	.34	1			
3	$^{27}Al(n,\alpha)^{24}Na$	0.006155	5.9	.28	.55	1		
4	$^{58}Ni(n,p)^{58}Co$	0.5298	4.1	.30	.63	.43	1	
5	$^{60}Ni(n,p)^{60}Co$	0.01750	3.7	.41	.62	.52	.46	1

[a]See Section III.F for a discussion of methods used to derive these results.
[b]Values are relative to ^{238}U neutron fission.

Table 24: Final Secondary Experimental Integral Cross-Section Ratios from the Present Investigation[a]

Reactions	Ratio	Ratio Error (%)
$^{7}Li(n,n't)^{4}He$-to-$^{27}Al(n,p)^{27}Mg$	5.113	4.5
$^{7}Li(n,n't)^{4}He$-to-$^{27}Al(n,\alpha)^{24}Na$	19.77	6.1
$^{7}Li(n,n't)^{4}He$-to-$^{58}Ni(n,p)^{58}Co$	0.2297	4.8
$^{7}Li(n,n't)^{4}He$-to-$^{60}Ni(n,p)^{60}Co$	6.954	4.2
$^{27}Al(n,p)^{27}Mg$-to-$^{27}Al(n,\alpha)^{24}Na$	3.867	5.0
$^{27}Al(n,p)^{27}Mg$-to-$^{58}Ni(n,p)^{58}Co$	0.04492	3.4
$^{27}Al(n,p)^{27}Mg$-to-$^{60}Ni(n,p)^{60}Co$	1.360	3.3
$^{27}Al(n,\alpha)^{24}Na$-to-$^{58}Ni(n,p)^{58}Co$	0.01162	5.6
$^{27}Al(n,\alpha)^{24}Na$-to-$^{60}Ni(n,p)^{60}Co$	0.3517	5.1
$^{60}Ni(n,p)^{60}Co$-to-$^{58}Ni(n,p)^{58}Co$	0.03303	4.1

[a]Derived from Table 23 results.

Table 25: Calculated Integral Cross-Section Ratios and Errors[a]

Reactions	Ratio	Ratio Error(%)
Primary Ratios:		
$^{7}Li(n,n't)^{4}He$-to-$^{238}U(n,f)$	0.1467	15.8
$^{27}Al(n,p)^{27}Mg$-to-$^{238}U(n,f)$	0.02871	11.3
$^{27}Al(n,\alpha)^{24}Na$-to-$^{238}U(n,f)$	0.007436	6.6
$^{58}Ni(n,p)^{58}Co$-to-$^{238}U(n,f)$	0.5043	7.4
$^{60}Ni(n,p)^{60}Co$-to-$^{238}U(n,f)$	0.02143	10.7
Secondary Ratios:		
$^{7}Li(n,n't)^{4}He$-to-$^{27}Al(n,p)^{27}Mg$	5.110	9.7
$^{7}Li(n,n't)^{4}He$-to-$^{27}Al(n,\alpha)^{24}Na$	19.73	16.5
$^{27}Al(n,p)^{27}Mg$-to-$^{27}Al(n,\alpha)^{24}Na$	3.861	12.4
$^{7}Li(n,n't)^{4}He$-to-$^{58}Ni(n,p)^{58}Co$	0.2909	13.2
$^{27}Al(n,p)^{27}Mg$-to-$^{58}Ni(n,p)^{58}Co$	0.05693	10.1
$^{27}Al(n,\alpha)^{24}Na$-to-$^{58}Ni(n,p)^{58}Co$	0.01475	9.6
$^{7}Li(n,n't)^{4}He$-to-$^{60}Ni(n,p)^{60}Co$	6.846	11.2
$^{27}Al(n,p)^{27}Mg$-to-$^{60}Ni(n,p)^{60}Co$	1.340	9.6
$^{27}Al(n,\alpha)^{24}Na$-to-$^{60}Ni(n,p)^{60}Co$	0.3470	11.7
$^{60}Ni(n,p)^{60}Co$-to-$^{58}Ni(n,p)^{58}Co$	~~0.04250~~ 0.04352	10.1

[a]Calculated using methods and numerical values described in Section IV.A.

Table 26: Twelve-Group Representation of the Zero-Degree Thick-Target $^{9}Be(d,n)^{10}B$ Neutron Spectrum at E_d = 7 MeV for Use in Determining Errors in Calculated Integral Cross-Section Ratios[a]

Group	Group Energy Limits (MeV)	Group[b] Fluence	Group Fluence Error (%)	Correlation Matrix											
				1	2	3	4	5	6	7	8	9	10	11	12
1	0.6 - 1.6	5.21	2.0	1											
2	1.6 - 2.6	6.19	2.0	0	1										
3	2.6 - 3.6	5.90	3.3	0	0	1									
4	3.6 - 4.6	4.79	4.3	0	0	.10	1								
5	4.6 - 5.6	3.87	6.2	0	0	.10	.59	1							
6	5.6 - 6.6	2.07	54.6	0	0	.10	.65	.85	1						
7	6.6 - 7.6	0.516	4.0	0	0	.11	-.23	-.35	-.45	1					
8	7.6 - 8.6	0.500	3.8	0	0	.11	.32	.38	.40	.14	1				
9	8.6 - 9.6	0.468	7.0	0	0	.06	.45	.58	.66	-.12	.45	1			
10	9.6 - 10.6	0.270	6.7	0	0	.06	.41	.52	.58	-.08	.43	.83	1		
11	10.6 - 11.6	0.150	18.5	0	0	.06	.62	.81	.95	-.36	.45	.79	.72	1	
12	11.6 - 12.6	0	0	0	0	.06	.06	.06	.33	.33	.33	.84	.84	.84	1

[a]Based on Ref. 12.
[b]Relative Values.

Table 27: Twelve-Group Representation of the ^{238}U Neutron-Fission Cross Section for Use in Determining Errors in Calculated Integral Cross-Section Ratios[a].

Group	Group Energy Limits (MeV)	Group Cross[b] Section (mb)	Cross-Section Error (%)	Correlation Matrix											
				1	2	3	4	5	6	7	8	9	10	11	12
1	0.6 - 1.6	28.9	7.5	1											
2	1.6 - 2.6	539.0	1.4	0	1										
3	2.6 - 3.6	523.0	2.5	0	0	1									
4	3.6 - 4.6	547.0	2.4	0	0	0	1								
5	4.6 - 5.6	536.0	2.6	0	0	0	0	1							
6	5.6 - 6.6	650.0	3.9	0	0	0	0	0	1						
7	6.6 - 7.6	935.0	3.9	0	0	0	0	0	1	1					
8	7.6 - 8.6	992.0	3.2	0	0	0	0	0	0	0	1				
9	8.6 - 9.6	997.0	3.2	0	0	0	0	0	0	0	1	1			
10	9.6 - 10.6	982.0	2.9	0	0	0	0	0	0	0	0	0	1		
11	10.6 - 11.6	987.0	2.9	0	0	0	0	0	0	0	0	0	1	1	
12	11.6 - 12.6	988.0	3.7	0	0	0	0	0	0	0	0	0	0	0	1

[a]Based on ENDF/B-V [16].

Table 28: Twelve-Group Representation of the $^{7}Li(n,n't)^{4}He$ Reaction Cross Section for Use in Determining Errors in Calculated Integral Cross-Section Ratios[a]

Group	Group Energy Limits (MeV)	Group Cross[b] Section (mb)	Cross-Section Error (%)	Correlation Matrix											
				1	2	3	4	5	6	7	8	9	10	11	12
1	0.6 - 1.6	0	0	1											
2	1.6 - 2.6	0	0	1	1										
3	2.6 - 3.6	0.621	104.0	0	0	1									
4	3.6 - 4.6	38.6	24.0	0	0	0	1								
5	4.6 - 5.6	122.0	8.3	0	0	0	.03	1							
6	5.6 - 6.6	364.0	9.0	0	0	0	0	.02	1						
7	6.6 - 7.6	374.0	3.8	0	0	0	.03	.11	.04	1					
8	7.6 - 8.6	374.0	4.0	0	0	0	.01	.03	.03	.18	1				
9	8.6 - 9.6	367.0	4.1	0	0	0	.01	.02	.02	.16	.18	1			
10	9.6 - 10.6	359.0	6.2	0	0	0	0	0	.06	.04	.05	.06	1		
11	10.6 - 11.6	349.0	9.8	0	0	0	0	.02	.01	.05	.06	.04	.04	1	
12	11.6 - 12.6	336.0	6.2	0	0	0	.01	.03	.02	.06	.05	.03	.02	.05	1

[a]Based on ENDF/B-V [16].

Table 29: Twelve-Group Representation of the $^{27}Al(n,p)^{27}Mg$ Reaction Cross Section for Use in Determining Errors in Calculated Integral Cross-Section Ratios[a]

Group	Group Energy Limits (MeV)	Group Cross[b] Section (mb)	Cross-Section Error (%)	Correlation Matrix											
				1	2	3	4	5	6	7	8	9	10	11	12
1	0.6 - 1.6	0	0	1											
2	1.6 - 2.6	5.23(-7)[b]	36.1	0	1										
3	2.6 - 3.6	2.01	19.1	0	.65	1									
4	3.6 - 4.6	7.50	13.4	0	.62	.59	1								
5	4.6 - 5.6	26.3	10.7	0	.62	.59	.56	1							
6	5.6 - 6.6	48.5	9.2	0	0	0	0	0	1						
7	6.6 - 7.6	69.7	10.7	0	0	0	0	0	.51	1					
8	7.6 - 8.6	87.3	15.0	0	0	0	0	0	0	0	1				
9	8.6 - 9.6	99.2	14.2	0	0	0	0	0	0	0	.67	1			
10	9.6 - 10.6	103.7	14.5	0	0	0	0	0	0	0	.67	1	1		
11	10.6 - 11.6	99.2	14.0	0	0	0	0	0	0	0	.69	.72	.72	1	
12	11.6 - 12.6	91.4	14.0	0	0	0	0	0	0	0	.69	.72	.72	1	1

[a]Based on ENDFB-V [16].

[b]5.23(-7) signifies 5.23×10^{-7}.

Table 30: Twelve-Group Representation of the $^{27}Al(n,\alpha)^{27}Mg$ Reaction Cross Section for Use in Determining Errors in Calculated Integral Cross-Section Ratios[a]

Group	Group Energy Limits (MeV)	Group Cross[b] Section (mb)	Cross-Section Error (%)	Correlation Matrix											
				1	2	3	4	5	6	7	8	9	10	11	12
1	0.6 - 1.6	0	0	1											
2	1.6 - 2.6	0	0	0	1										
3	2.6 - 3.6	0	0	0	0	1									
4	3.6 - 4.6	1.42(-8)[b]	24.5	0	0	0	1								
5	4.6 - 5.6	0.0125	11.4	0	0	0	.58	1							
6	5.6 - 6.6	2.14	7.8	0	0	0	.63	.54	1						
7	6.6 - 7.6	18.0	7.2	0	0	0	.68	.59	.64	1					
8	7.6 - 8.6	44.2	6.7	0	0	0	.73	.63	.69	.74	1				
9	8.6 - 9.6	72.7	5.8	0	0	0	.70	.60	.66	.71	.77	1			
10	9.6 - 10.6	92.9	5.6	0	0	0	.73	.63	.69	.75	.80	.77	1		
11	10.6 - 11.6	109.0	5.6	0	0	0	.73	.63	.69	.75	.80	.77	1	1	
12	11.6 - 12.6	122.0	5.0	0	0	0	0	0	0	0	0	0	0	0	1

[a]Based on ENDF/B-V [16].
[b]1.42(-8) signifies 1.42×10^{-8}.

Table 31: Twelve-Group Representation of the $^{58}Ni(n,p)^{58}Co$ Reaction Cross Section for Use in Determining Errors in Calculated Integral Cross-Section Ratios[a]

Group	Group Energy Limits (MeV)	Group Cross[b] Section (mb)	Cross-Section Error (%)	Correlation Matrix											
				1	2	3	4	5	6	7	8	9	10	11	12
1	0.6 - 1.6	2.55	14.1	1											
2	1.6 - 2.6	52.4	10.3	0	1										
3	2.6 - 3.6	208.0	10.3	0	1	1									
4	3.6 - 4.6	372.0	7.1	0	.34	.34	1								
5	4.6 - 5.6	480.0	7.1	0	.34	.34	1	1							
6	5.6 - 6.6	568.0	7.1	0	.34	.34	.50	.50	1						
7	6.6 - 7.6	595.0	7.1	0	.34	.34	.50	.50	1	1					
8	7.6 - 8.6	599.0	7.1	0	.34	.34	.50	.50	.50	.50	1				
9	8.6 - 9.6	599.0	7.1	0	.34	.34	.50	.50	.50	.50	1	1			
10	9.6 - 10.6	587.0	11.2	0	.22	.22	.32	.32	.32	.32	.32	.32	1		
11	10.6 - 11.6	570.0	11.2	0	.22	.22	.32	.32	.32	.32	.32	.32	1	1	
12	11.6 - 12.6	542.0	15.8	0	.15	.15	.22	.22	.22	.22	.22	.22	.14	.14	1

[a]Based on ENDF/B-V [16].

Table 32: Twelve-Group Representation of the $^{60}Ni(n,p)^{60}Co$ Reaction Cross Section for Use in Determining Errors in Calculated Integral Cross-Section Ratios[a]

Group	Group Energy Limits (MeV)	Group Cross[b] Section (mb)	Cross-Section Error (%)	Correlation Matrix											
				1	2	3	4	5	6	7	8	9	10	11	12
1	0.6 - 1.6	0	0	1											
2	1.6 - 2.6	0	0	0	1										
3	2.6 - 3.6	2.51(-4)[b]	7.6	0	0	1									
4	3.6 - 4.6	0.612	7.6	0	0	1	1								
5	4.6 - 5.6	11.0	7.6	0	0	1	1	1							
6	5.6 - 6.6	32.8	12.5	0	0	.38	.38	.38	1						
7	6.6 - 7.6	65.8	12.5	0	0	.38	.38	.38	1	1					
8	7.6 - 8.6	98.4	10.8	0	0	.44	.44	.44	.27	.27	1				
9	8.6 - 9.6	138.0	10.8	0	0	.44	.44	.44	.27	.27	1	1			
10	9.6 - 10.6	175.0	10.3	0	0	0	0	0	0	0	0	0	1		
11	10.6 - 11.6	124.0	10.3	0	0	0	0	0	0	0	0	0	1	1	
12	11.6 - 12.6	149.0	10.3	0	0	0	0	0	0	0	0	0	1	1	1

[a]Based on ENDF/B-V [16].

[b]2.51(-4) signifies 2.51×10^{-4}.

Table 33: Components of the Calculated Integral Cross-Section Ratio Errors[a]

Reactions		Error Components (%)			
σ_1	σ_2	σ_1[b]	σ_2[c]	$\sigma_1+\sigma_2$[d]	ϕ[e]
$^{238}U(n,f)$	$^{7}Li(n,n't)^{4}He$	1.0	4.5	4.6	15.1
$^{238}U(n,f)$	$^{27}Al(n,p)^{27}Mg$	1.0	6.3	6.4	9.3
$^{238}U(n,f)$	$^{27}Al(n,\alpha)^{24}Na$	1.0	5.5	5.6	3.5
$^{238}U(n,f)$	$^{58}Ni(n,p)^{58}Co$	1.0	6.0	6.0	4.3
$^{238}U(n,f)$	$^{60}Ni(n,p)^{60}Co$	1.0	7.0	7.1	8.0
$^{27}Al(n,p)^{27}Mg$	$^{7}Li(n,n't)^{4}He$	6.3	4.5	7.7	5.8
$^{27}Al(n,\alpha)^{24}Na$	$^{7}Li(n,n't)^{4}He$	5.5	4.5	7.1	14.9
$^{27}Al(n,\alpha)^{24}Na$	$^{27}Al(n,p)^{27}Mg$	5.5	6.3	8.4	9.2
$^{58}Ni(n,p)^{58}Co$	$^{7}Li(n,n't)^{4}He$	6.0	4.5	7.5	10.9
$^{58}Ni(n,p)^{58}Co$	$^{27}Al(n,p)^{27}Mg$	6.0	6.3	8.7	5.1
$^{58}Ni(n,p)^{58}Co$	$^{27}Al(n,\alpha)^{24}Na$	6.0	5.3	8.1	5.1
$^{60}Ni(n,p)^{60}Co$	$^{7}Li(n,n't)^{4}He$	7.0	4.5	8.3	7.4
$^{60}Ni(n,p)^{60}Co$	$^{27}Al(n,p)^{27}Mg$	7.0	6.3	9.4	1.8
$^{60}Ni(n,p)^{60}Co$	$^{27}Al(n,\alpha)^{24}Na$	7.0	5.5	8.9	7.5
$^{58}Ni(n,p)^{58}Co$	$^{60}Ni(n,p)^{60}Co$	6.0	7.0	9.2	4.1

[a]Ratio=(Response of Reaction σ_2) ÷ (Response of Reaction σ_1).
[b]Error in ratio due only to reaction σ_1.
[c]Error in ratio due only to reaction σ_2.
[d]Error in ratio due to reactions σ_1 and σ_2, combined.
[e]Error in ratio due only to spectrum ϕ.

Table 34: Neutron-Source Comparisons

Neutron Source	Principal Reaction	Maximum Neutron Energy (MeV)	Zero-Degree[a] Neutron Yield (n/sr/μC)	$^{58}Ni(n,p)^{58}Co$ σ(mb)[b]	$^{58}Ni(n,p)^{58}Co$ Response[c]	$^{60}Ni(n,p)^{60}Co$ σ(mb)[b]	$^{60}Ni(n,p)^{60}Co$ Response[c]
7.6-MeV protons on a 200-keV-thick natural Li metal target	$^{7}Li(p,n)^{7}Be$	< 5.9	1.2(7)[d]	< 550	< 6.6(9)	< 25	< 3(8)
7.6-MeV deuterons on a 2-cm long gas target filled to 2 atmospheres with D_2	$^{2}H(d,n)^{3}He$	< 10.7	1.4(8)	~ 580	~ 8.1(10)	< 120	< 1.7(10)
7.6-MeV deuterons on a thick Be target	$^{9}Be(d,n)^{10}B$	< 12	3.6(10)	~ 240	~ 8.6(12)	~ 10.4	~ 3.7(11)

[a]Based on data from Ref. 40.

[b]Approximate cross section for the indicated neutron field, based on data from Refs. 12 and 16.

[c]Response = (Zero-degree neutron yield) × σ. This parameter indicates relative reaction yield to be expected, under otherwise comparable conditions, for irradiation in the indicated neutron field.

[d]1.2(7) signifies 1.2×10^{7}.

FIGURE CAPTIONS

Figure 1: Schematic diagram of the thick-beryllium-target assembly and the fission-detector apparatus used for irradiations in the present experiment.

Figure 2: Plots of the spectrum (ϕ), the differential cross section (σ), and the response ($\sigma\phi$) for the various reactions of interest in the present investigation.

Figure 3: Schematic comparison of measured and calculated integral reaction-cross-section ratios. All results are plotted relative to the experimental results. The horizontal bars indicate uncertainties. Solid bars represent experimental results. They are centered on unity as they must be by definition. The open bars represent the calculated results. The vertical marks located at the centers of the open bars identify the calculation-to-experiment ratio values (C/E) for the corresponding physical quantities listed at the left margin.

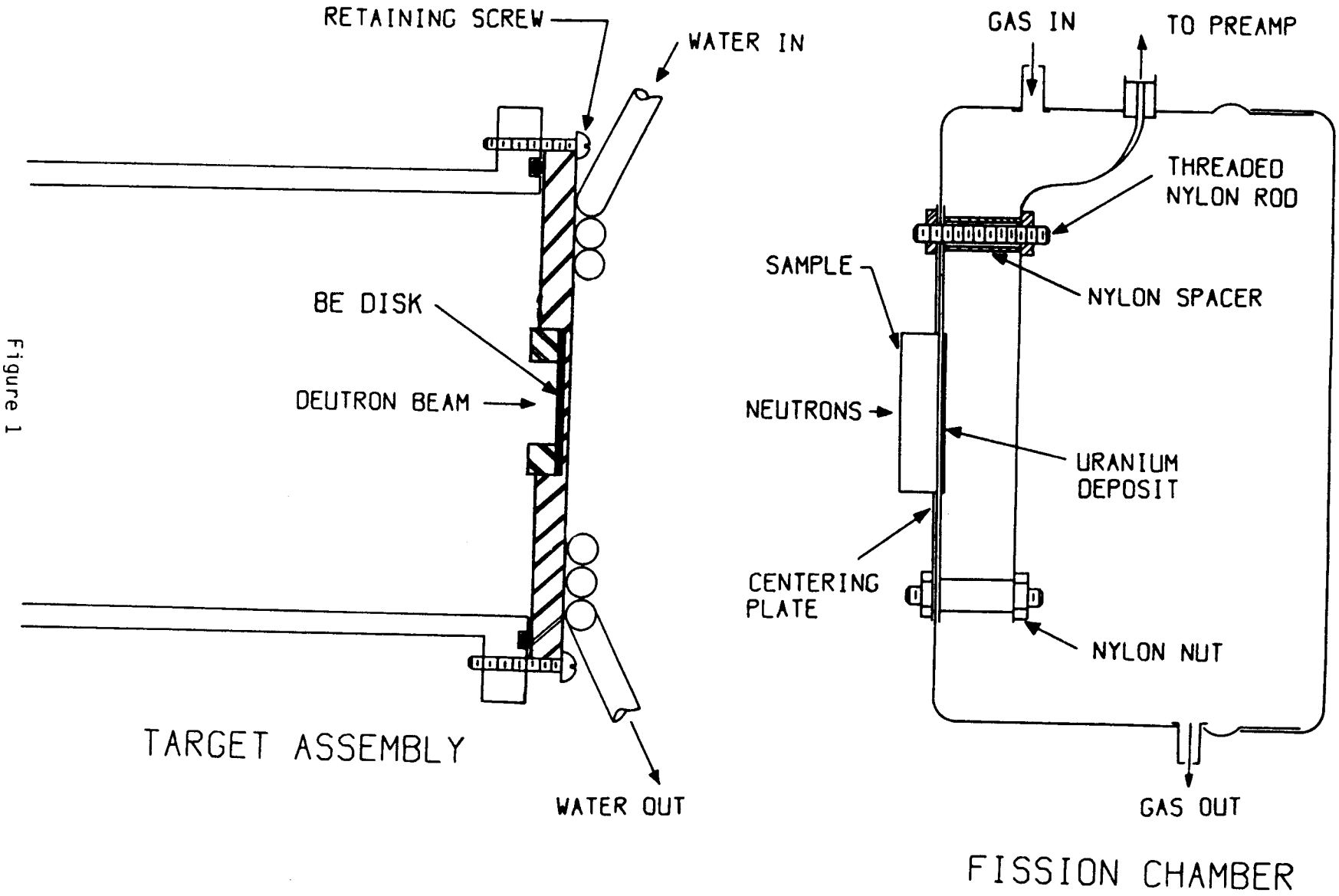
RETAINING SCREW
WATER IN
BE DISK
DEUTRON BEAM
WATER OUT
TARGET ASSEMBLY
GAS IN
TO PREAMP
THREADED
NYLON ROD
SAMPLE
NYLON SPACER
NEUTRONS
URANIUM
DEPOSIT
CENTERING
PLATE
NYLON NUT
GAS OUT
FISSION CHAMBER

Figure 1

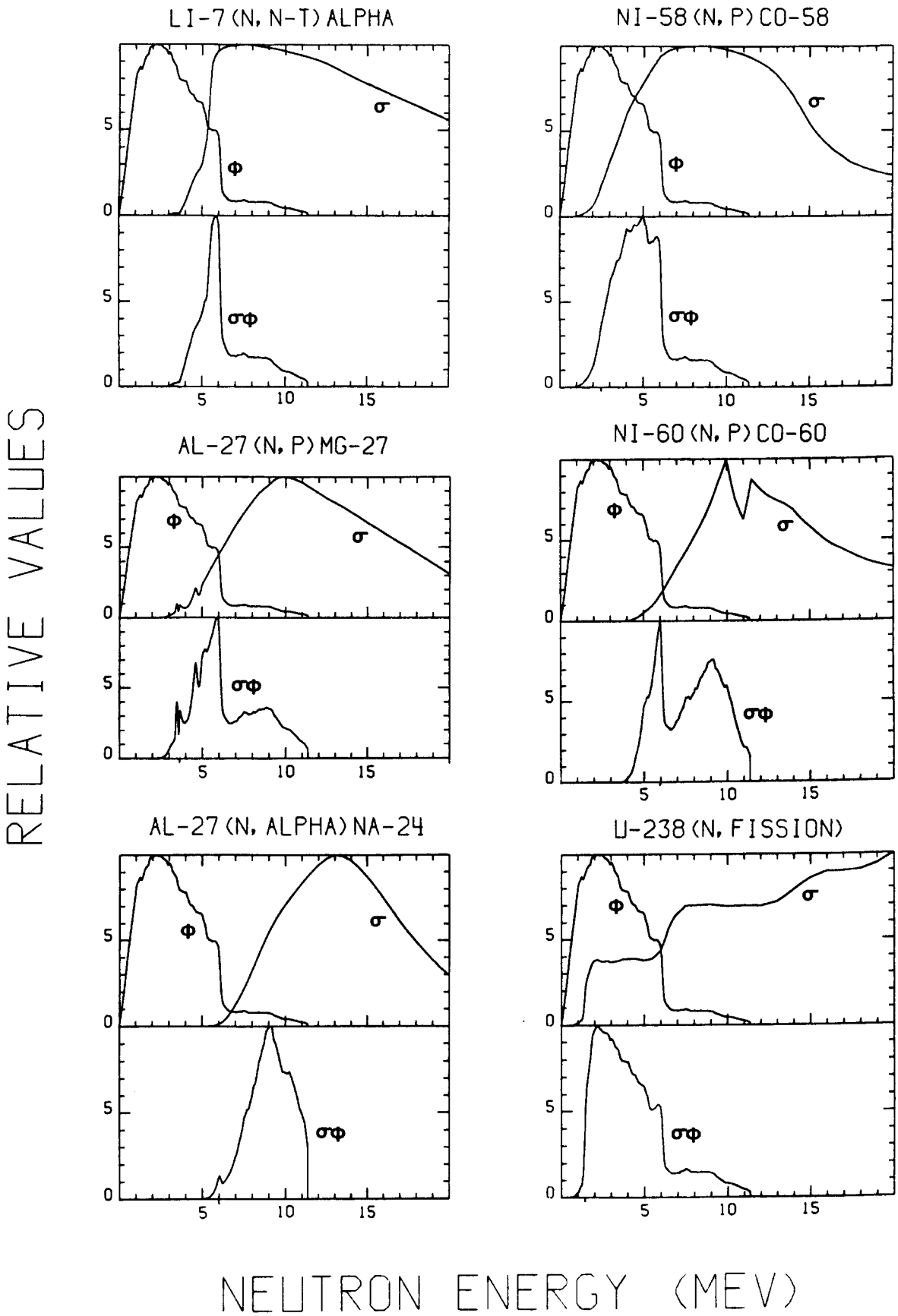
LI-7 (N, N-T) ALPHA
NI-58 (N, P) CO-58
AL-27 (N, P) MG-27
NI-60 (N, P) CO-60
AL-27 (N, ALPHA) NA-24
U-238 (N, FISSION)
Φ
σ
σΦ
0
5
10
15
RELATIVE VALUES
NEUTRON ENERGY (MEV)

Figure 2

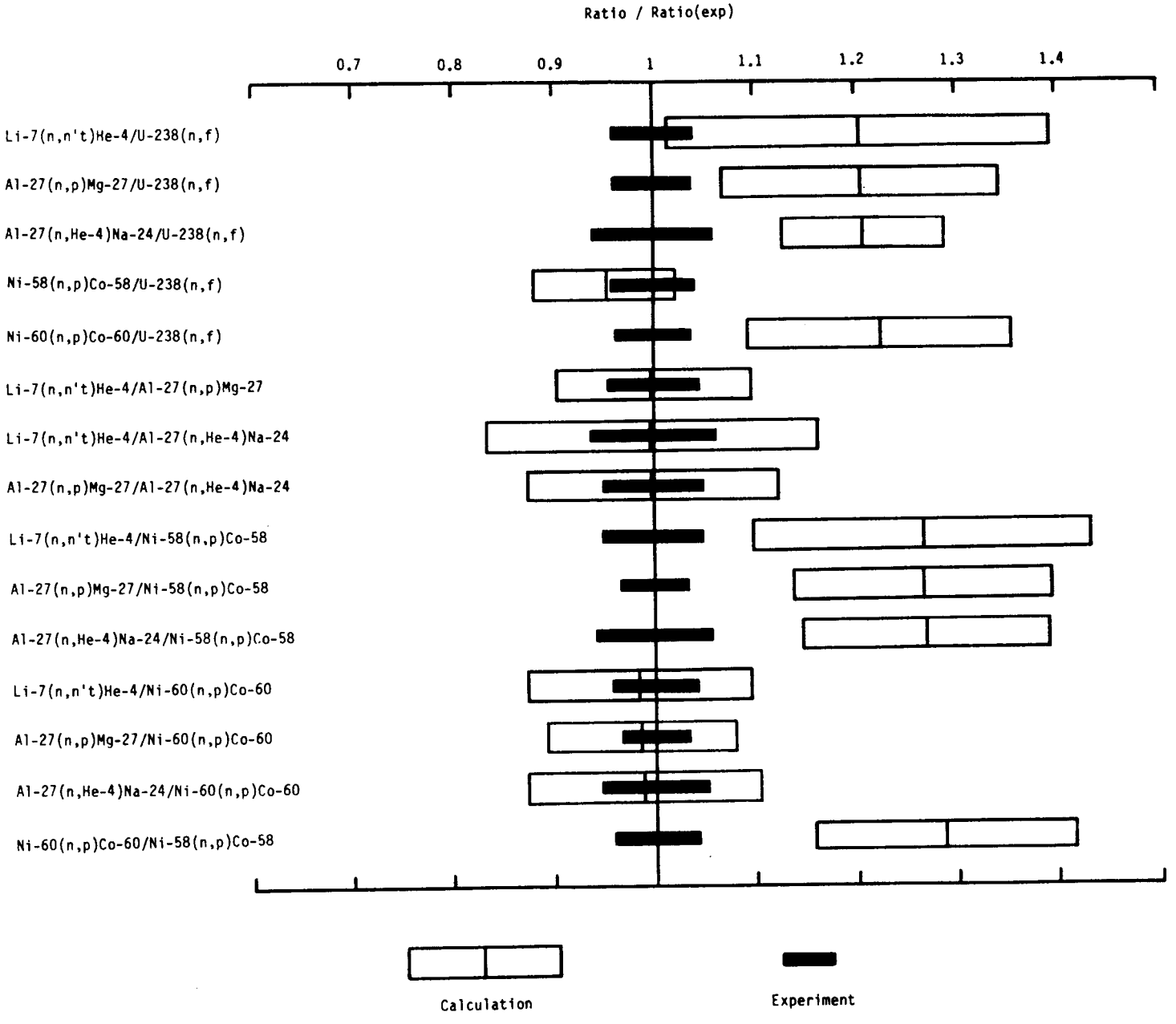
Ratio / Ratio(exp)
0.7
0.8
0.9
1
1.1
1.2
1.3
1.4
Li-7(n,n't)He-4/U-238(n,f)
Al-27(n,p)Mg-27/U-238(n,f)
Al-27(n,He-4)Na-24/U-238(n,f)
Ni-58(n,p)Co-58/U-238(n,f)
Ni-60(n,p)Co-60/U-238(n,f)
Li-7(n,n't)He-4/Al-27(n,p)Mg-27
Li-7(n,n't)He-4/Al-27(n,He-4)Na-24
Al-27(n,p)Mg-27/Al-27(n,He-4)Na-24
Li-7(n,n't)He-4/Ni-58(n,p)Co-58
Al-27(n,p)Mg-27/Ni-58(n,p)Co-58
Al-27(n,He-4)Na-24/Ni-58(n,p)Co-58
Li-7(n,n't)He-4/Ni-60(n,p)Co-60
Al-27(n,p)Mg-27/Ni-60(n,p)Co-60
Al-27(n,He-4)Na-24/Ni-60(n,p)Co-60
Ni-60(n,p)Co-60/Ni-58(n,p)Co-58
Calculation
Experiment

Figure 3